

Chapter 4: Multi Band Behavior, Optical, and Electronic Properties in IV-VI materials

4.1 - Introduction

In this chapter, I will give a detailed account of my work in the IV-VI materials (PbTe, PbSe, PbS, and SnTe). Because this family of materials has been extensively studied since the 1950's, an account of some of the historical findings along with the current state of the field will be outlined. My contribution comes in largely in the context of band engineering in these materials, both through optimization of the electronic properties (SnTe, PbSe/SrSe alloys) and through determining the nature and effects of the temperature-dependent shifts in the band structure which are known result in improved performance at high temperatures.

Even though there is a wealth of historical work on the lead and tin chalcogenides over the last 60 years, the topic has received resurging interest over the last few years. This is largely due to the newly established method for measuring the thermal conductivity: the Laser Flash Apparatus (LFA, discussed in Chapter 2). LaLonde et al. reports that some of the more commonly cited zT estimates for the lead chalcogenides did not explicitly measure the high temperature thermal properties; rather, they were extrapolated from a room temperature lattice thermal conductivity and a high temperature resistivity (using the Wiedemann-Franz law)—this resulted in an overestimation in κ of ~30% [110]. In fact, the LFA method (even though it was available beginning in the 1960's) was not widely applied to the lead chalcogenides until recently. With the combination of optimal doping levels and the more modern and accurate method for measuring the thermal conductivity at high temperatures it has been found that optimally doped binary PbTe can reach zT of up to ~1.4 for n-type and up to 1.5 for p-type at high temperatures; the modern result is nearly double that of many of the 1960's measurements. Since then, many groups around the world have been reporting high zT values, many even higher than the doped binary samples

through alloying with other elements. Recent reports on PbTe and its alloys have suggested an extraordinarily high peak zT of between 1.0 and 2.2 in the temperature range useful for waste heat recovery depending on the specific dopant and alloy [18, 28, 34, 111-113].

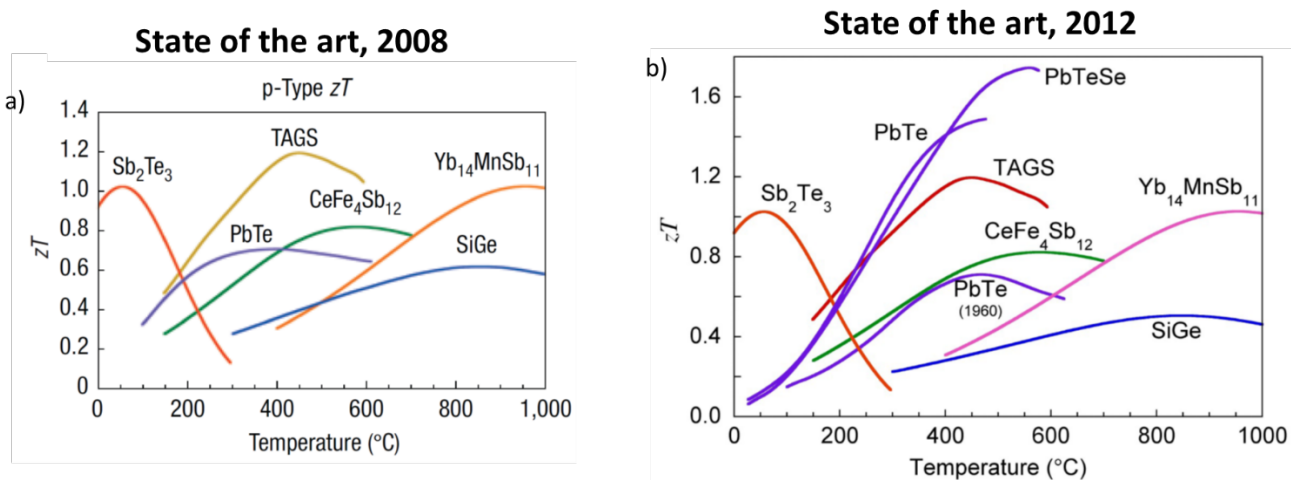


Figure 4-1: Illustration of the rapidly changing state of the thermoelectrics field which until ~2010 believed that the optimum in zT was much less than 1.0. a) was taken from [114], and b) from [110].

4.2 - Lead Chalcogenides, Band Engineering, and Band Convergence

While optical properties measurements are commonly used for characterizing semiconducting materials, electronic measurements are much more commonly performed for thermoelectric materials (neglecting optical properties). This is likely because the goal is to produce a large zT , but not necessarily to understand the electronic structure which produced it. In this section, I will apply a combination of optical and *ab-initio* computational analyses to understand the electronic band positions in the lead chalcogenides, particularly how they change as a function of temperature. Multiple band effects have been identified as being responsible for enhancing thermoelectric properties; I will thoroughly review the literature on this topic in the lead chalcogenides as well as provide insight using a combination of optical properties, electronic properties, and *ab-initio* calculations.

4.2a - Lead Chalcogenide Literature Review

In p-type PbTe a complex valence band structure exists that has been described with two valence bands: a lighter band at the L point (direct) and a heavier along the Σ line in the Brillouin zone [15, 16, 58, 85, 86, 115-120] as shown in a later chapter (Figure 7-1). The enhanced thermoelectric efficiency in PbTe is attributed to valley degeneracy arising from band convergence, which yields higher thermopower without greatly reducing carrier mobility [16]. The region of electronic states along the Σ line has been described and modeled as a separate, heavy band, even though recent work suggests that it may be associated with the band at L [91, 117, 121]. However, two-band transport analysis, e.g., when both bands are considered separately, is consistent with most experimental observations and is useful for rational thermoelectric material design; therefore, in this chapter we will refer to these states as a separate band at Σ [15, 16, 18, 122]. Based on historical evidence [123-125] and calculations [84, 86, 91, 117], the band extremum at Σ is believed to lie about 0.1 – 0.15 eV below that of the band at L at room temperature (See Figure 1-3 and Figure 4-2). Still, the exact band energies and their temperature dependence continue to be disputed [16, 91, 117, 121]. The other IV-VI materials are known to have larger L - Σ offsets of approximately 0.25 [126, 127], 0.5 [126], and 0.4 [128-130] eV for PbSe, PbS, and SnTe at room temperature, respectively. The band offset in all of the IV-VI materials is known to be temperature dependent, and the primary and secondary valence bands are thought to move towards each other at a rate of $\sim 2 - 4 \times 10^{-4}$ eV/K [16, 27, 39, 60, 87]. Both the temperature dependence and the offset can be modified through alloying with a variety of elements (cation: Sr, Ca, Mg, Mn or anion: S, Se, Te) [15-18, 21, 25, 42, 131], often resulting in very good performance. While several groups have discussed nano/micro-structuring to improve thermoelectric performance [12, 21, 131, 132], which is generally thought to be a result of reduction of thermal conductivity through additional phonon scattering, a fully optimized thermoelectric material will likely require some combination of alloying/nano-microstructure to

benefit from the effects of reduced thermal conductivity as well as band engineering. Furthermore, it is important to be able to separate the nano-structuring effects in order to better quantify them; in this thesis I will be focusing on understanding the electronic band structure and band engineering in these materials and I will therefore avoid samples which have detectable amounts of precipitates (nano or otherwise). Knowledge of the specific band offset and its temperature dependence in these materials is crucial since band convergence is thought to be responsible for the improved thermoelectric properties. Hence, this work is motivated by the hope that a more accurate understanding of the electronic band structure can provide a clearer route forward to band structure engineering in the lead chalcogenides for further improvement of zT .

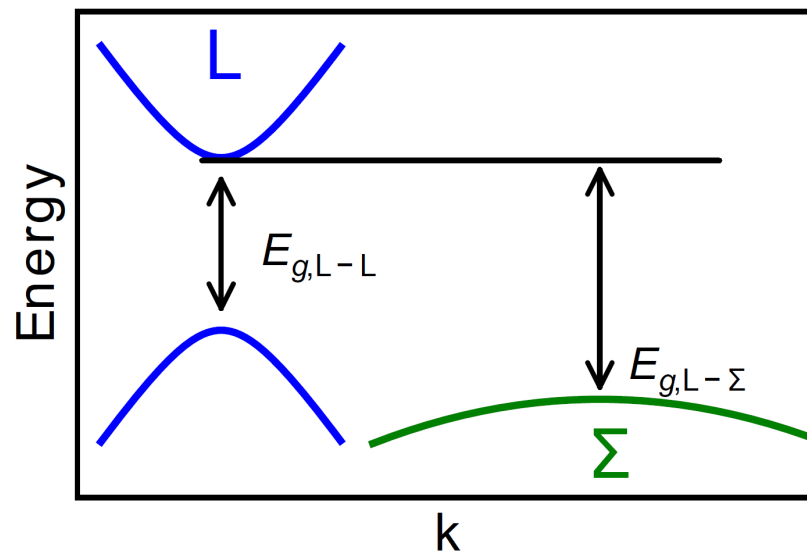


Figure 4-2: Schematic representation of the L and Σ band extrema in PbX (X=Te, Se, S) and SnTe (as presented in previous work[126]).

Electrical and magnetic measurements have been performed previously to characterize the energy band structure, including estimates of the valence band offsets and their temperature dependence [115, 121, 123-125, 133-137]. Nevertheless, interpretation of the results depends upon transport models. Optical absorption edge spectroscopy in semiconductors is a more direct route to obtain information about electronic states near the band edge (E_g), which can be used in conjunction with transport models to experimentally map out the electronic structure.

Historically, optical data on the PbX materials have been plentiful. Early data from the 1950's and 60's [27, 36-39, 74, 75, 138-149] provided a good foundation for both the low temperature [27, 38], room temperature [37, 38, 74], and temperature dependent band gaps [27, 36, 39, 141, 143, 145] are widely cited in the field. Many works since then have aimed to perform more careful characterization of the IV-VI materials and their alloys [41, 42, 81, 148, 150-153], including estimates of the valence band offset (though interband-valence band absorption [38, 90]), additional comments on the origin of their temperature-dependence [87, 154], band non-parabolicities [151], possible resonant/impurity states with In [155-157] and Tl [157, 158], and some helpful reviews [60]. As mentioned in Chapter 2, many of the previous reports of optical band gap measurements on PbTe have used single crystal samples measured in transmission [27, 36-42], which, in many cases, limited their maximum measureable absorption coefficients. Spectroscopic ellipsometry can bypass the necessity for the Kramers-Kronig analysis by measuring both the real and imaginary components of the dielectric function simultaneously, and some studies of lead chalcogenides as photodetectors or infrared lasers use these techniques [159, 160].

Regarding thermoelectric efficiency, the main point that comes into question for these materials is their $L-\Sigma$ band offset, temperature dependent shifts in ΔE , and the temperature at which the bands are effectively converged, T_{cvg} . The most widely cited article that reports T_{cvg} for the lead chalcogenides is one of the earlier reports by Tauber et al. in 1966 [27] indicating a plateau in the indirect band gap at approximately 400 K for PbTe (Gibson et al. observe the plateau for all of the lead chalcogenides around this temperature [36]). The band offset and convergence temperature supposed by Tauber et al. has been widely used in the field and has been supported by other evidence, including a peak in the Hall coefficient at around this temperature [16, 135]. However, recent work points out some discrepancies in the literature data [91, 121]: poor resolution of the early optical data (Miller et al. have a resolution of 7 meV [161]),

improper extrapolation of the absorption edge (often incorrectly assumed to be indirect [27, 161]), and that a wide range of values for $\frac{d\Delta E}{dT}$ (where ΔE is the offset between the L and Σ bands) that are reported from $2 - 4 \times 10^{-4} \frac{eV}{K}$. In order to help resolve some of these questions, I have performed measurements using diffuse reflectance infrared Fourier transform spectroscopy (DRIFTS) on polycrystalline samples for the lead chalcogenides over a broad range of temperatures; I compare the results to *ab initio* molecular dynamics (AIMD) calculations to study the temperature dependent gap and examine the band structure at high temperatures.

The positive temperature coefficient of the band gap in lead chalcogenides, unlike many common semiconductors, is favorable for thermoelectric materials. An increasing gap with temperature can act to suppress bipolar effects caused by intrinsic carrier activation, increasing the optimum zT . The temperature dependent gap in PbX is known to be due to both lattice expansion and electron-phonon interactions [39, 87, 162]. The effect can be described by:

$$\frac{dE_g}{dT} = \left(\frac{dE_g}{dT}\right)_V - 3\alpha_L K_B \left(\frac{dE_g}{dP}\right)_T \quad \text{Equation 4-1}$$

where α_L is the linear thermal expansion coefficient $\left(\frac{1}{L^*} \left(\frac{dL^*}{dT}\right)_P\right)$, K_B is the bulk modulus $\left(-\frac{1}{V} \left(\frac{dV}{dP}\right)_T\right)$, $\left(\frac{dE_g}{dT}\right)_V$ describes the electron-phonon interactions, and $\left(\frac{dE_g}{dP}\right)_T$ is the band gap dependence on pressure [39, 60, 87]. Prakash et al. performed detailed pressure dependent optical measurements to determine that $\left(\frac{dE_g}{dP}\right)_{T=300K}$ was equal to -9.15, -9.1, and -7.4×10^{-6} eV/bar for PbS, PbSe, and PbTe respectively. This measurement is comparable with *ab-initio* calculated figures obtained in a more recent reference, which obtained -6.85×10^{-6} eV/bar for PbTe [163]. Prakash estimated that the electron-phonon interaction term $\left(\frac{dE_g}{dT}\right)_V$ was approximately 40%, 40%, and 60% of the overall change in dE_g/dT for PbS, PbSe, and PbTe, respectively.

4.2b - Results

AIMD Calculations

In order to probe the effects of temperature on the electronic bands, I took a two-pronged approach involving both temperature-dependent optical measurements and *ab-initio* calculations performed by our collaborators Hyunchul Kim and Massoud Kaviani (University of Michigan). *Ab-initio* molecular dynamics (AIMD) calculations combine electronic structure calculations (DFT) with molecular dynamics (MD) calculations. While *ab-initio* calculations are inherently performed at $T=0$ K (no lattice vibrations, simply minimizing the energy of the system), MD allows us to simulate how a material might actually look at high temperature by allowing the atomic positions to move from their equilibrium values. Snapshots are taken once the computed temperature is equal to the desired one, and a DFT calculation is performed on the perturbed supercell. By performing AIMD simulations coupled with DFT band structure calculations on supercells, we were able to calculate the effect of the thermal motion of the atoms in PbX on both the direct (L) and indirect (Σ) band gaps, the results of which are shown in Figure 4-3 (points and solid lines). For all of the lead chalcogenides, the direct ($L-L$) band gap increases from low temperature with a slope (dE_g/dT) that decreases as temperature is increased. The indirect ($L-\Sigma$) gap increases at a slower rate with temperature for PbTe, but decreases with temperature in PbSe and PbS, resulting in a convergence temperature (T_{cvg}) of about 700, 900, and 1000 K for PbTe, PbSe, and PbS, respectively. The dashed line in Figure 4-3 represents the effect of lattice expansion alone; it is clear that both electron-phonon interaction and lattice expansion make significant contributions to dE_g/dT . The electron-phonon contribution does appear to grow weaker as the temperature increases for all materials in comparison to contributions to dE_g/dT due to expansion only. Still, in the absence of electron-phonon interactions, the bands would not converge until a temperature greater than the melting point of PbX. Hence, the presence of electron-phonon interactions, exclusive to AIMD calculations, is required in order predict band convergence at the

temperatures that we observe experimentally. In comparison to Prakash's estimate, we obtain that the portion of the electron-phonon contribution to dE_g/dT , $\left(\frac{dE_g}{dT}\right)_V$, is 37%, 41%, and 67% for PbS, PbSe, and PbTe, respectively, all of which agree well with Prakash's estimates [39]. Furthermore, our calculations show that the gap at Σ changes relatively little (particularly in PbTe) and that band convergence is primarily the result of electron-phonon interaction on the L bands.

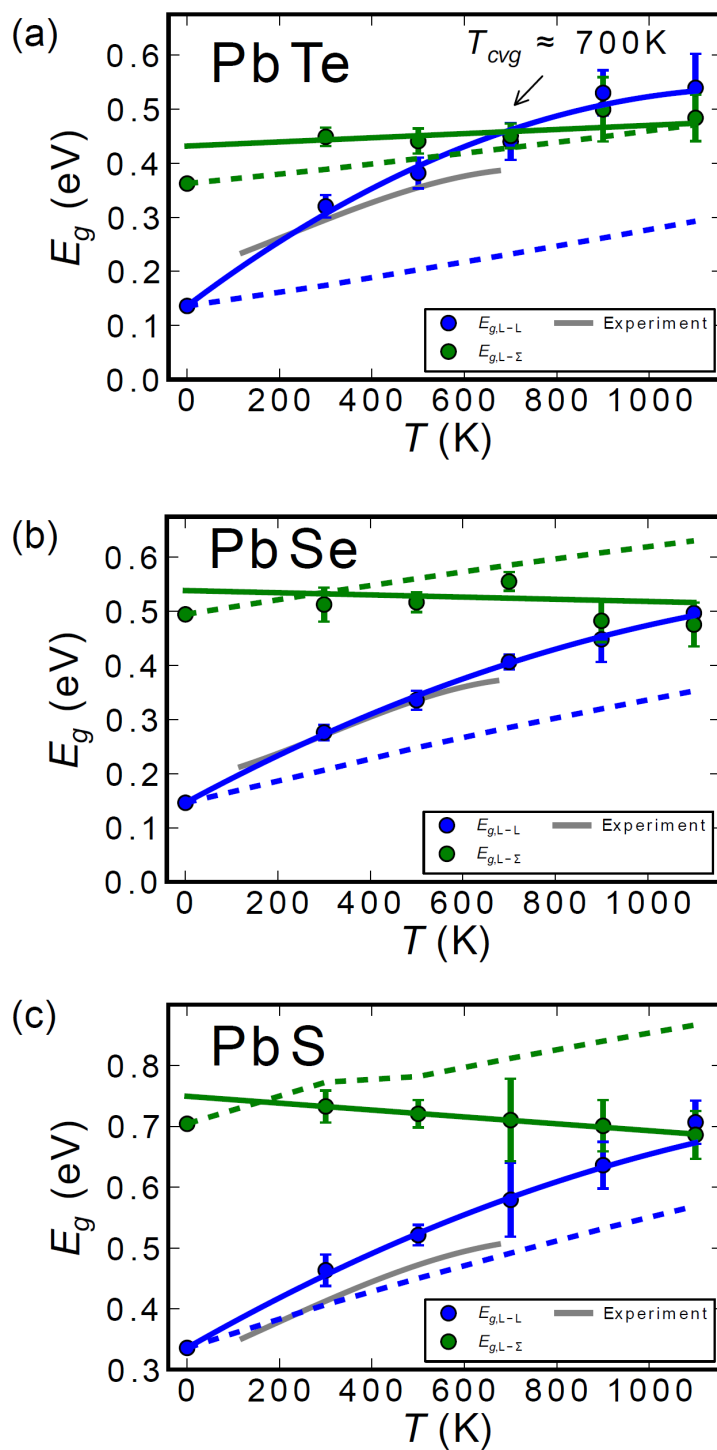


Figure 4-3: AIMD calculated temperature dependent band gap for a) PbTe, b) PbSe, and c) PbS. Circular points represent the computed (electron-phonon + expansion) average value over several snapshots (along with the error bar plotted as a standard deviation), and solid lines represent a guide to the eye. Dashed lines show the change in band gap when electron-phonon interactions are not considered (thermal expansion only). The grey line indicates a best fit to the experimental result.

Experimental results are also obtained in the form of temperature dependent optical absorption spectra (Figure 4-4a). It should be noted that undoped samples were measured in order to avoid the Burstein Moss shift and other complexities that are encountered when trying to interpret optical results in doped samples (as detailed in Chapter 3). Figure 4-4b and c show the extrapolated direct gaps, as well as reported values from the literature. A linear fit of the changing gap up to 500 K returns a value for $dE_g/dT = 3.2 \pm 0.1$ (10^{-4} eV / K), which is almost the same for all PbX (X=S, Se, Te). Several works report a value for dE_g/dT in the range 3.0 to 4.9×10^{-4} eV/K [27, 36, 39, 87, 140, 164, 165], although generally the values are on the higher end of this range. In agreement with the references, the rate of change is mostly linear from low temperature (100 K) to room temperature and does not vary depending on the particular chalcogen atom. However, the actual band gap value depends on how it is obtained from the absorption edge. In addition to the value of the band gap, its temperature dependence is important because of what it implies about the relative positions of L and Σ extrema and their contributions to the thermoelectric properties, which optical band gap measurements have played a role in determining [27].

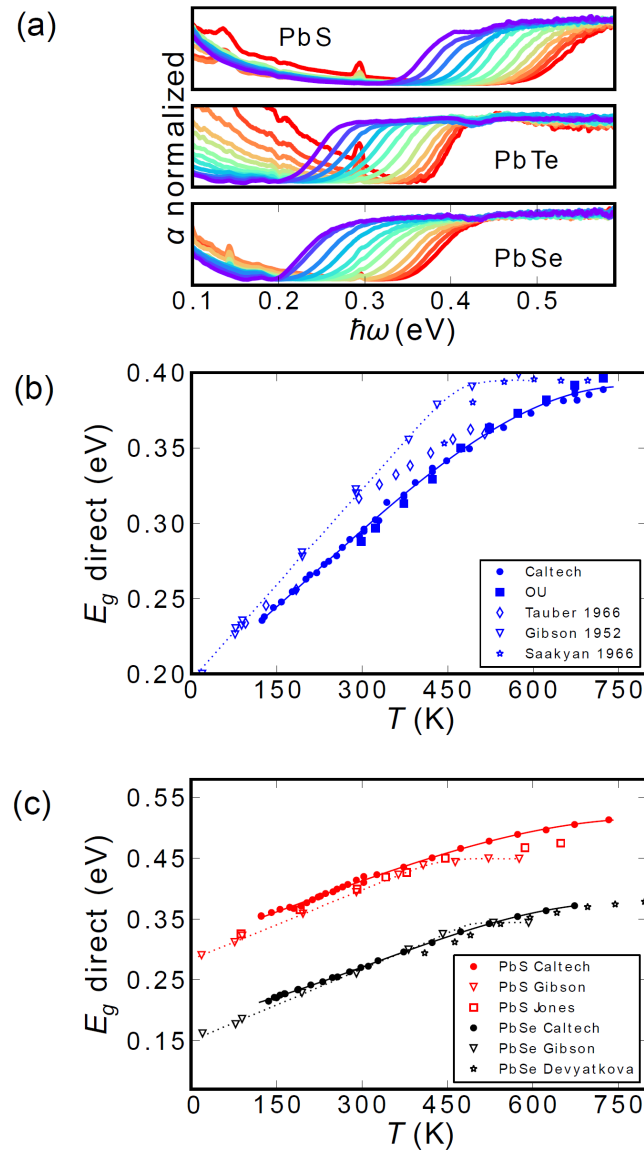


Figure 4-4: a) Temperature-dependent optical absorption spectra for PbS, PbTe, and PbSe. b) Extrapolated direct band gap as a function of temperature for PbTe measured at Caltech, OU (University of Oklahoma), Tauber et al. [27], Gibson et al. [36], and Saakyan et al. [166]. c) Extrapolated results for PbSe and PbS measured at Caltech along with references from Jones et al. [143] and Devyatkova et al [136].

4.2c - Discussion, Impact, and interpretation of the results

As mentioned previously, both Gibson (1952) and Tauber (1966) both showed an increasing band gap that stopped changing above 400 K [27, 36]. Tauber interpreted this as a shifting primary valence band (which is now known as a direct gap at the L point) that is replaced by the secondary valence band (Σ) above 400 or 500 K in PbTe. Tauber's work is widely cited as

evidence of the convergence temperature, T_{cvg} , in PbTe. Band convergence, however, does not require a plateauing optical band gap. Direct transitions (L - L) have been shown to be 10-100x as strong as indirect ones, which require both photon and phonon participation [48]. In fact, without sufficient separation between the indirect and direct gaps, it may be difficult to distinguish the smaller indirect absorption edge from the exponential Urbach tail (an exponential tail in density of states into the band gap resulting from impurities and disorder in the material, discussed in Chapter 3.2b). Consequently, we expect that the temperature dependent optical band gap should continue to increase even if the L and Σ bands had converged—suggesting that Tauber's aforementioned results cannot be used as direct evidence of L and Σ valence band convergence. Upon re-extrapolating the Tauber et al. absorption spectra (which was necessary since only indirect transitions were fit) using Tauc extrapolation, the resulting band gaps do continue to increase, contrary to the conclusions of Gibson and Tauber. Our results, shown in Figure 4-4b and c, show that the optical gap continues to increase for temperatures greater than 673 K, albeit at a lower rate above 500 K. In fact, several other authors have observed no plateau in the band gap via optical measurements in PbTe [154, 167], PbSe [127], and PbS [143]; however, these articles are not generally cited in more modern investigations. In this thesis, both experimental and AIMD results suggest that the band convergence temperature is much higher than 400 K, suggested by Gibson and Tauber et al., and that T_{cvg} is actually closer to 700 K in PbTe.

The temperature dependence of electronic transport properties (resistivity, Hall effect, and Seebeck) can also be used to estimate the band gap. Devyatkova and Saakyan et al. [136, 166] (also shown in Figure 4-4b and c) measured the electronic/thermoelectric properties of both n and p-type samples in the bipolar regime to estimate the temperature dependent gap using an extrapolation technique for the single parabolic band model. They obtained a constant gap for temperatures greater than 550 K in PbTe and one that increased continuously until 800 K in PbSe. These estimates seem to be consistent with results from this work, although both calculation and

optical measurement from this work suggest a somewhat higher convergence temperature. This may be a result of the fact that effective convergence (as in the bands are within a few $k_B T$ of each other and both contribute significantly to transport) can occur at temperatures lower than the true convergence temperature, which will be discussed in detail in Figure 4-6a-c.

The question of whether the absorption edge can provide evidence of band convergence is an interesting one that is of great importance for both the scientific community and this thesis. Usually, one will make a Tauc plot scaled to the appropriate power in order to determine whether a material shows direct or indirect transitions (as outlined in Chapter 2). This is usually determined by fitting the linear portion of the appropriate Tauc plot and extrapolating back to zero absorption. In the case of the lead chalcogenides, however, this simple exercise seems to yield confusing results. Part of the reason that many of the early works on the subject concluded that PbX had an indirect band gap is because the absorption edges (even though we know that the primary band gap is direct) give good linear extrapolation fits for both direct and indirect gaps. This has been observed and discussed by a few authors [37, 39] who provide different explanations. Because the extrapolated indirect gap usually falls ~ 0.02 - 0.05 eV below the extrapolated direct one, Scanlon et al. proposed that the indirect edge could be a result of $k=0$ phonons imparting their energy (but not their wave vector) to the excited electron, resulting in some indirect contribution to the $L-L$ direct gap transitions [37]. Prakash tends to believe that this linear indirect region is actually a coincidental fit in the region between the Urbach edge, and the direct absorption edge [39]. Regardless, of who is correct, it is necessary to understand why Tauber and Gibson's data yields a maximum in band gap. We suspect that it may be related to the fact that both Gibson and Tauber et al. used optical transmission through relatively thick samples, limiting the maximum measurable absorption coefficient to hundreds of cm^{-1} . Combined with an increasing baseline absorption coefficient as temperature increases, Gibson and Tauber were only observing the very bottom of the absorption spectrum at high temperatures. DRIFTS, however, seems to measure a

broader range of absorption coefficient. To test this hypothesis, we will consider both the direct and indirect extrapolations (Figure 4-5). Due to the nature of the transformations, direct transition extrapolations tend to favor higher absorption coefficients (absorption coefficient is squared), while indirect ones tend to enhance the lower magnitude absorption coefficient.

In order to investigate whether the assumption of direct gap may have resulted in overlooking the indirect $L-\Sigma$ gap, I have plotted the extrapolation for both the direct and indirect gaps as a function of temperature for each of the lead chalcogenides in Figure 4-5. Here we can see that the temperature-dependent slope of the indirect and direct gaps are very close to the same values in all of the lead chalcogenides, indicating that the two extrapolations are intimately linked. In order to determine whether the indirect $L-\Sigma$ band gap actually becomes the primary one, we would be looking for some break in this pattern, perhaps a maximum in the indirect gap as observed by Tauber (while the direct one continues to grow). However, in all of the lead chalcogenides, both the direct and indirect extrapolations seem to change together, with the only exception being the very highest PbTe data points; between 350 and 400°C the direct gap seems to grow more slowly than the indirect gap—resulting a nearly constant indirect gap. While this could indicate that the indirect, $L-\Sigma$ gap is becoming the primary one for PbTe above these temperatures, a single data point does not constitute a trend. Further, the sample could not be taken to temperatures much higher than ~400°C because of significant evaporation that quickly coated the windows. Therefore, we have concluded that all of the lead chalcogenides show direct-gap behavior over the entire temperature range (up to 400°C) with no evidence of indirect transitions becoming the primary ones. This finding is consistent with the AIMD calculations, but differs from Gibson and Tauber's conclusions, which we attribute to their low maximum measurable absorption coefficients due to a relatively large sample thickness measured in transmission.

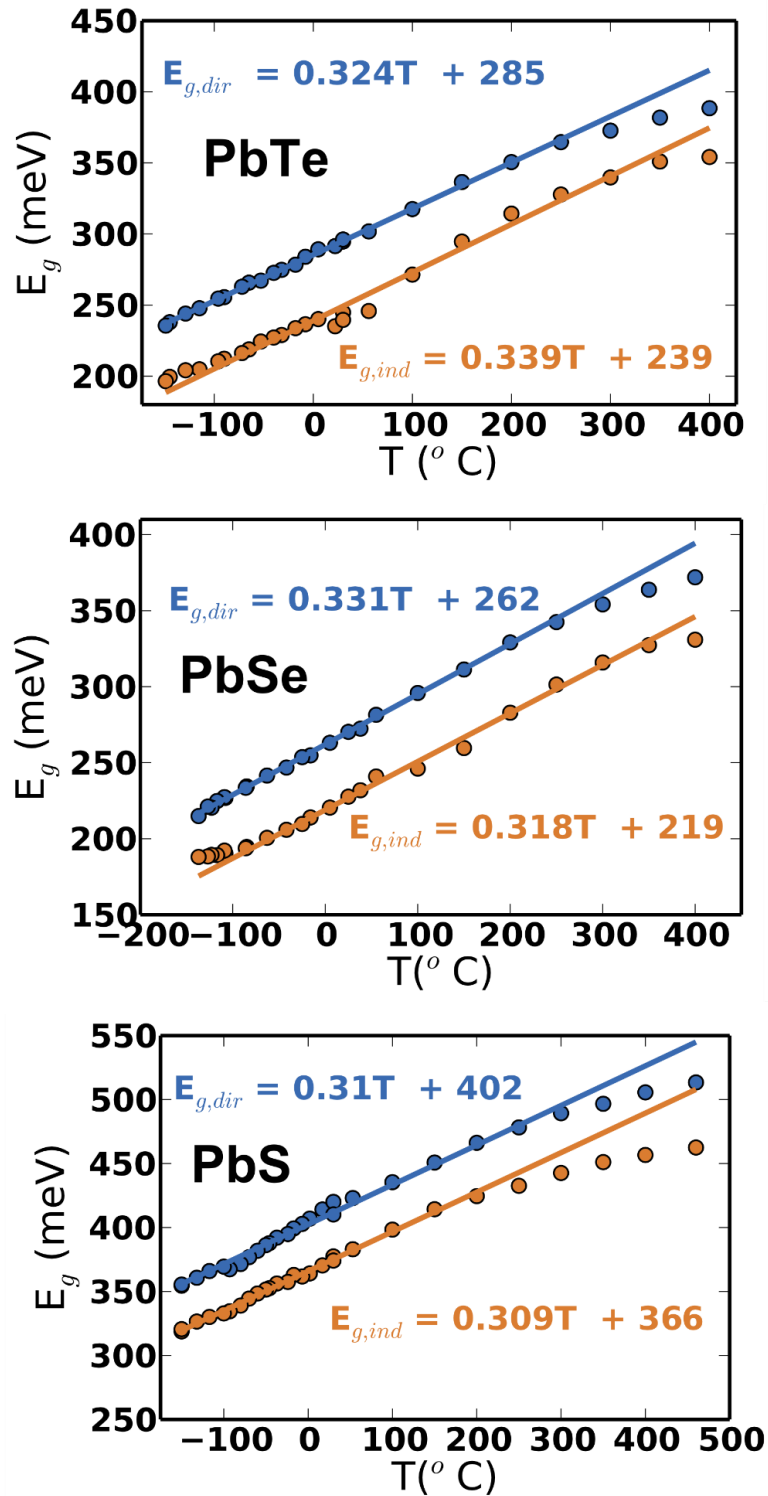


Figure 4-5: Temperature dependent band gap for the direct (dir) and indirect (ind) extrapolations of the absorption edge along with linear fits as functions of temperature for PbTe, PbSe, and PbS.

The implications that a higher T_{cvg} has on other conclusions about the temperature dependent band structure of PbTe are that the temperature-dependent $L-\Sigma$ offset should be reconsidered. Historically, valence band offsets in PbX samples have been determined by intra and inter-valence band free carrier absorption measurements with photon energies less than the fundamental gap [74, 90, 116]; this is an experimental method for determining the $L-\Sigma$ energy offset directly. Values of $2-4 \times 10^{-4}$ eV/K were reported for the temperature dependence of the offset between the two valence bands using these techniques [90, 127], which approximately agree with estimates from transport properties [121]. However, the range of values mean that the answer is still an open one. Several methods of estimating the $L-\Sigma$ offset (ΔE) and T_{cvg} are available, including free carrier absorption, band gap measurements as shown in this work (which can be used to indirectly infer the inter-valence band behavior), and temperature-dependent electronic transport properties.

As an example of how electronic transport measurements have been used to estimate the band offset, it has been suggested that a peak in the Hall resistance with temperature implies band convergence and can be used as an estimate of T_{cvg} [15, 16, 123, 124]. Interestingly, these results show a peak around 450 K for p-type PbTe, consistent with the T_{cvg} estimate of Tauber et al. However, as pointed out by Jaworski et al., this represents the temperature at which the conductivity of carriers in either band are equal and not necessarily when the bands are at the same energy [121]. We tested this hypothesis using a two valence band transport model consistent with Pei et al [16] with a different band convergence temperature (consistent with the 3.2×10^{-4} eV/K, convergence at 700 K and a slightly lower L-band effective mass of $0.26 m_0$). We modeled a Hall coefficient peak at around 450 K (approximately where the L and Σ band conductivities are equal), even though the band convergence does not occur until 700 K. This result suggests that a higher convergence temperature is not in conflict with the Hall coefficient peak observed around 450 K.

While this study shows that the band convergence temperature is higher than previously believed, it also confirms that such a convergence should indeed occur at high temperatures. However, just because the actual convergence may not occur until 700 K in PbTe, this does not mean that the electronic transport properties will not reflect contributions from the Σ band at lower temperatures. It is understood that electronic transport properties are determined by the bands within $3-4 k_B T$ of the chemical potential. This means that effective convergence can occur when the L and Σ bands are within this energy-range of each other. In order to illustrate effective convergence, I plot the projected Fermi distribution along with the calculated temperature-dependent Fermi distribution in Figure 4-6 a-c. In this figure, we see a lower effective convergence temperature of ~ 600 , 800 , and 850 K for PbTe, PbSe, and PbS, respectively, consistent with the observations of high zT in these materials at high temperatures.

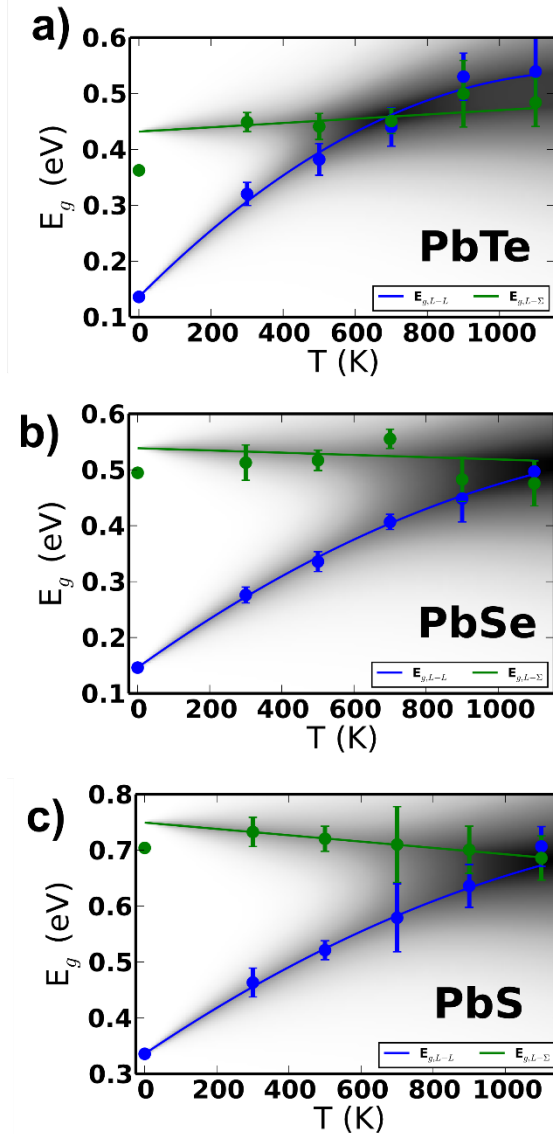


Figure 4-6: Calculated temperature dependent gap between either the L or Σ valence bands and L conduction bands for a) PbTe, b) PbSe, and c) PbS with temperature-dependent Fermi distribution overlaid indicating that the region of effective convergence occurs at temperatures below the actual T_{cvg} .

4.2d - Conclusions

While electronic transport models have used band convergence temperatures of 400-500 K to adequately describe the transport properties in PbTe [16], a higher convergence temperature is not necessarily inconsistent with these results. The observance of effective convergence at ~ 600 K indicates that the effect of the Σ band is still significant for transport in binary PbTe. Optical absorption edge data show an increasing optical gap with temperature at a rate of $\sim 3.2 \times 10^{-4}$ eV/K

for all three lead chalcogenides up to 500 K (whereas the slope above that is smaller and steadily decreasing). AIMD calculations deduce that about half of the contribution is due to lattice expansion, while the rest is due to electron-phonon interaction. Contrary to prior temperature dependent optical absorption literature, this work suggests that the optical gap continues to increase for temperatures up to 673 K. While previous work used the E_g plateau in PbTe as evidence of the convergence temperature, our results suggest that the plateau does not occur at such low temperatures. Optical absorption and AIMD DFT calculations in this work both suggest that the band convergence in PbTe occurs at about 700K a temperature higher than concluded previously. Future sections of this thesis will focus on strategies for enhancing thermoelectric properties through band convergence by alloying.

4.2e - Methods

Optical characterization for this section was done using DRIFTS. Direct and indirect extrapolations of the optical band gaps were performed using the Tauc method as described in detail in Chapter 2.

AIMD simulations were performed by my collaborator Hyouchul Kim and Massoud Kaviani of the University of Michigan to describe the effects of temperature on the band structures of the lead chalcogenides according to the methods described in a previous work[162]. The temperature-dependent lattice dynamics were calculated using AIMD considering the Fermi-Dirac smearing factor and the thermally expanded lattice parameter from experimental results: $a(T) = 6.422 + (0.9545 \times 10^{-4})T + (2.615 \times 10^{-8})T^2$ [168]. Calculations were performed on large supercells (54 atoms) and the near edge band positions were averaged over three snapshots per temperature. In the calculations of band gap energy as a function of temperature, we only consider the maxima of the valence and conduction bands at the L and Σ points in the band structure. This is done to exclude some band splitting and shifting. We note that above-mentioned choices (data averaging of several snapshots and the different calculation schemes) result in a spread of values

for which error bars are plotted. Sample synthesis details are given both in Chapter 2 and in the original paper on this topic [126].

4.3 - Band Engineering and Band Convergence through Alloying in the Lead Chalcogenides

4.3a - Introduction

Thermoelectric performance in the lead chalcogenides has proved to be among the best of any potential thermoelectric material in the 600K – 800K range. As mentioned previously, many attempts at engineering the electronic band structure in PbTe and other IV-VI materials have been successful at improving the thermoelectric properties [15-17, 21, 25, 131, 169, 170]. In this section, I will highlight a successful band engineering attempt in PbSe by alloying with SrSe, which I did in collaboration with my colleagues Heng Wang and Yoshiki Takagiwa [25]. Alloying in this case improves the properties by pushing the valence bands closer together (as a result of the widening L-L band gap), which we observe through electronic/optical properties and computed *ab-initio* density of states.

In PbSe and PbTe, the secondary valence band maximum (along the Σ line of the Brillouin zone) contributes significantly to the thermoelectric performance at high temperatures [58, 127, 136, 166]. The best thermoelectric performance is found around temperatures where the two valence bands are converged (within a few $k_B T$ of one another) [16, 26]. For PbTe the convergence temperature (T_{cvg}) has been shown in the previous section to be around 700 K (with effective convergence occurring above ~ 600 K—Figure 4-6a). In PbSe, the Σ band is further away [127, 171] (~ 0.25 eV at 300 K) from the primary band maximum at L, resulting in a higher T_{cvg} (~ 900 K, ~ 800 K for effective convergence; Figure 4-6). Early works [58, 137, 172, 173] based on Hall coefficient data confirm this result, suggesting a T_{cvg} around 750 K for binary PbSe. In order

to enhance thermoelectric performance in PbSe, it is beneficial to reduce T_{cvg} by tuning the secondary valence band position; in this section we accomplish this by alloying with SrSe.

One strategy that has been successful at reducing ΔE in PbTe [14, 15] has been alloying with alkaline-earth chalcogenides (MgTe) that also have the rock salt crystal structure and wide band gaps. Previous results have shown that it is possible to grow $Pb_{1-x}Sr_xSe$ thin films via molecular beam epitaxy (MBE) where the lattice constant changes gradually following the Vegard's law; this is accompanied by a tunable band gap in a wide range with different SrSe content [174-176]. Given the rock-salt structure and the lattice parameter of 6.25 Å for SrSe, it is highly probable that an appreciable solubility of SrSe in PbSe in the bulk material could exist as well. In addition, recent studies regarding thermoelectric PbTe with SrTe addition resulted in a noticeable thermal conductivity reduction without significantly impairing the carrier mobility [14, 120], indicating that SrSe in PbSe may yield beneficial alloying results as well.

4.3b - Results and Discussion

A series of PbSe/SrSe samples were synthesized with varying sodium (p-type) dopant concentration. SrSe is very effective in changing the band energies in PbSe. As shown in Figure 4-7a and Figure 4-8, the optical band gap (as determined from the absorption edge) of undoped $Pb_{1-x}Sr_xSe$ alloys is noticeably larger than that of PbSe. Band gaps of the alloys increase approximately linearly with Sr content up to 12%, resulting in a band gap that is nearly double that of pure PbSe. The change of band structure consequently affects the transport properties. Figure 4-7d shows measured room temperature Seebeck coefficient as function of Hall carrier density (the Pisarenko relation). For PbSe, due to the large offset between two valence-band maxima at room temperature, the contribution from the secondary Σ band on transport is negligible and the Pisarenko relation (data in black squares) can be explained with a single band model [177] (black curve) using L valence band parameters determined previously [65]. With the addition of Sr, S starts to deviate from the curve at high doping levels, resulting in higher values compared to pure

PbSe given the same carrier density. Among the $\text{Pb}_{1-x}\text{Sr}_x\text{Se}$ alloys, the Seebeck coefficient also increases as the Sr content increases. When considering the origin of the increasing Seebeck coefficient, one possibility is that it is due to increasing L -band effective mass. However, if the increased S were simply due to a larger effective mass, the value would be proportionally larger at all n_H ; in this case, however, the low n_H $\text{Pb}_{1-x}\text{Sr}_x\text{Se}$ samples seem to converge with pure PbSe curve. Instead, we attribute the deviation from the single band model (the black curve) at high n_H by considering the contribution from the heavier (Σ) band as the Fermi level moves deeper into the valence band, as is commonly observed in heavily doped p-type PbTe [34]. The continuous change in the direct L - L band gap due to SrSe alloying can explain the gradual change of Pisarenko relation. If the energy of the L valence band is reduced as the band gap increases and this reduces the band offset in PbSe between L and Σ valence bands (meaning $\frac{dE_{g,L-L}}{dx} > \frac{dE_{g,L-\Sigma}}{dx}$), the secondary Σ band will play a more noticeable role in heavily doped, Sr containing PbSe, consistent with our observed Seebeck Pisarenko plot.

In accordance with a literature observation [176] on thin films samples at 77 K, we assume that the L and Σ valence band offset (ΔE) changes as approximately half of the L - L band gap change with strontium content ($\frac{d\Delta E}{dx} = \frac{1}{2} \frac{dE_{g,L-L}}{dx}$), as shown in (Figure 4-7e, inset). Using this assumption, the calculated Pisarenko relation for each $\text{Pb}_{1-x}\text{Sr}_x\text{Se}$ alloy can be calculated as shown in Figure 4-7d (solid curves); the resulting two-band transport model curves are in reasonable agreement with the observed experimental Seebeck results over a wide range of chemical potentials (Na doping concentrations).

In addition to shifting the electronic band structure, alloying reduces the electronic and thermal conductivity due to point defect scattering. Figure 4-7b shows the reduction in lattice thermal conductivity as Sr is added (point defect scattering of phonons) at 300 and 850 K. This reduction is often thought to be beneficial for thermoelectric materials, but only if the thermal

conductivity is reduced more than the electronic mobility [178]. In this case, the electronic mobility is reduced by more than 50% relative to the undoped sample, meaning that disorder is likely not beneficial to thermoelectric properties in this series of samples.

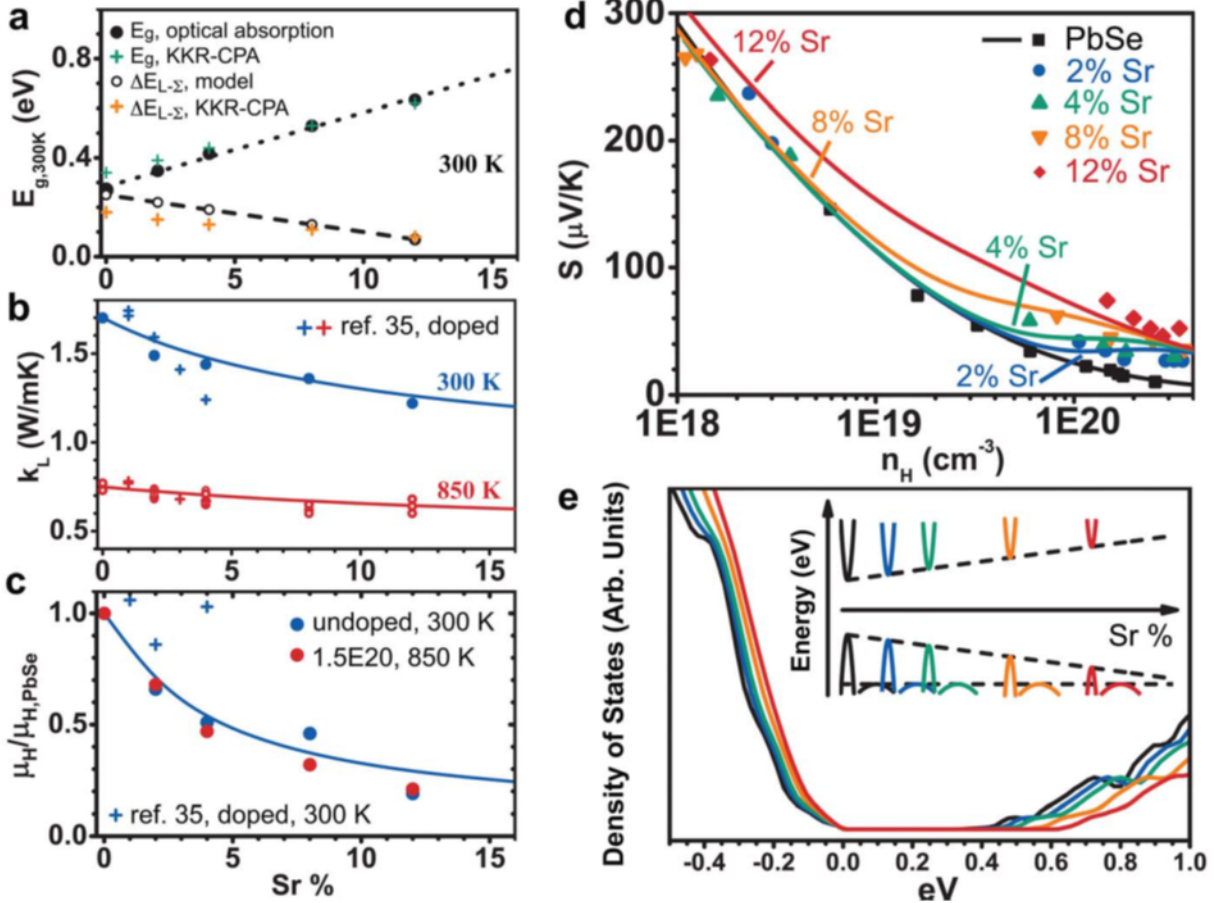


Figure 4-7: a) The measured band gap E_g and the proposed energy separation between two valence bands $\Delta E_{L-\Sigma}$ of $Pb_{1-x}Sr_xSe$ alloys, each is consistent with calculated values. b) Lattice thermal conductivity as function of Sr content at 300 K and 850 K. 300 K values are from undoped samples. c) Normalized Hall mobility as function of Sr content for undoped samples at 300 K and doped samples with same carrier density at 850 K. d) Pisarenko relation of p-type PbSe and $Pb_{1-x}Sr_xSe$ alloys. Lines are calculated using the proposed band model. e) The calculated DOS spectrum of $Pb_{1-x}Sr_xSe$ alloys; kinks in DOS around -0.1 eV are used to estimate $\Delta E_{L-\Sigma}$, and the inset illustrates the proposed band model, which is also given in (a).

The optical absorption edge in the binary lead chalcogenides begins with direct transitions across the fundamental gap at the L point. Because these direct transitions do not require phonon participation, they are believed to dominate the absorption spectra compared with the $L-\Sigma$ indirect transitions which should occur at higher energies. This limits traditional optical absorption to accurately determining the direct (fundamental) gap (while missing any $\Sigma-L_c$ indirect transitions).

While inter-valence band optical transitions (Σ - L_v) have been observed and used to estimate the valence band offset in older Russian literature [127], this method requires some analysis to subtract free carrier absorption contributions; however, we did not observe any inter-valence band transitions in this system that might indicate the valence band offset. Instead, we employed *ab-initio* calculations of the electronic band structure to determine how it might change with Sr content. My collaborator, Yoshiki Takagiwa, performed first principle calculation using the Korringa-Kohn-Rostoker Green function formalism under the coherent potential approximation[179-181] (KKR-CPA). The KKR-CPA method is a powerful tool for visualizing the electronic density of states (DOS) for disordered materials without establishing a supercell; this technique is widely used in studies of thermoelectrics to imitate random substitutions [105, 182-184]. Calculated DOS spectra of $\text{Pb}_{1-x}\text{Sr}_x\text{Se}$ confirmed both the increase of band gap and the decrease of energy separation between L and Σ bands. These are shown in Figure 4-7 a and e; the results are consistent with regards to the proposed model.

Because of the widening band gap in the PbSe/SrSe alloys, it is possible that the indirect (L - Σ) optical transition might be observable in the optical absorption edge. In the previous section, I showed that even at the highest temperatures I was not able to directly detect the Σ band in any of the pure lead-chalcogenide absorption edges. I present the room temperature optical absorption results along with various transformations of the data in Figure 4-8. The normalized absorption spectra show a steady shift upwards in the absorption edge (as represented in Figure 4-7a) as the strontium content is increased. Along with a shift of the absorption edge to higher energies, the onset of the absorption edge does appear to broaden as the strontium content is increased. Because it is possible that the longer absorption edge tail to low energies is a result of some indirect L - Σ transitions, we need to consider this possibility. The indirect extrapolation is shown in Figure 4-8c, which does show regions of linearity. In fact, the samples with the three largest Sr content (4, 8, and 12%) show two linear regions (potentially consistent with indirect

optical absorption associated with absorption/emission of a phonon [43]). However, I believe that it is actually related to disorder due to increased randomness in the alloy, as evidenced by the Urbach edge plotted in Figure 4-8b. By taking the logarithm of the absorption data, exponential features, such as the Urbach absorption edge (discussed in Chapter 3), should appear linear. In this case, we can clearly see the evolution of the Urbach edge, which goes from being quite small in pure PbSe ($x=0$) to stretching over nearly 0.15 eV in the sample with 12% Sr. This fits well with the supposition of Prakash (mentioned in the previous section) that the observation of a linear region for the indirect extrapolation is simply a coincidental fit resulting from the transition from the exponential Urbach edge to the direct extrapolation [39]. For all alloys the absorption spectra are consistent with direct transitions, which I attribute to the L-L gap as in pure PbSe [171]. It is possible that upon investigating the temperature-dependent gap that these features might arise.

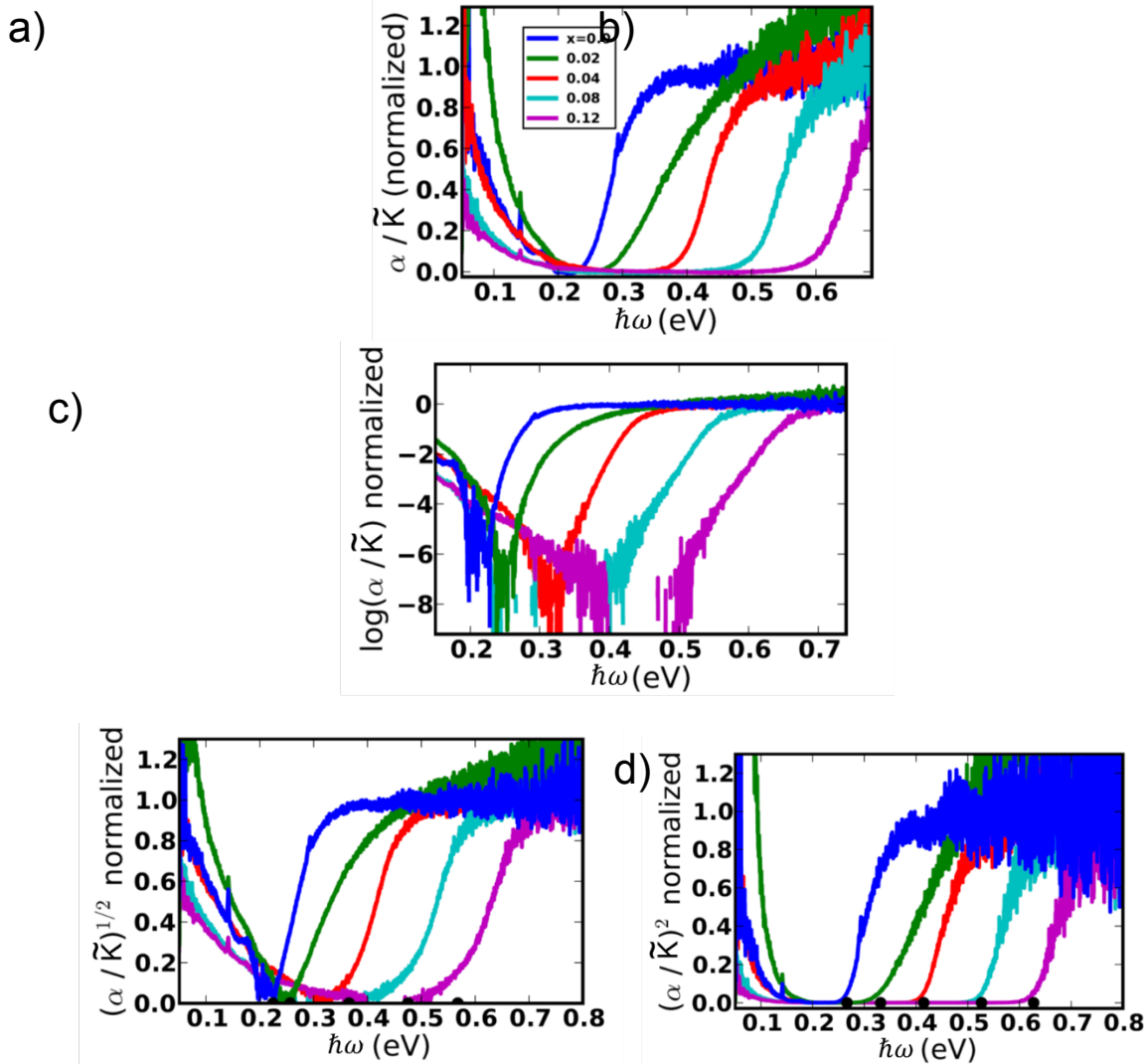


Figure 4-8: Optical data over a series of $(\text{PbSe})_{1-x}/(\text{SrSe})_x$ samples at room temperature—showing a) the normalized Kubelka Munk function, b) the log of the normalized Kubelka Munk function, c) the indirect extrapolation of the normalized Kubelka Munk function, and d) the direct extrapolation. Black dots on the axes indicate the extrapolated values.

The temperature dependent extrapolated direct band gap for each of the Sr-alloyed samples (and pure PbSe) is plotted in Figure 4-9 along with literature data from Shen et al. [174]. Our results are in good agreement with the literature values (which tended to be measured at low temperatures). Perhaps the most significant finding here is that the temperature coefficient (dE_g/dT) seems to decrease as Sr is added. This may be one of the reasons that, even at high temperatures, it is difficult to observe the indirect transition (because the Σ band never overtakes L as the primary valence band). It is important to note, however, that just because the secondary

band is not observable using optical properties, the transport properties of doped samples do reflect the increased valley degeneracy and effective mass of the secondary Σ band.

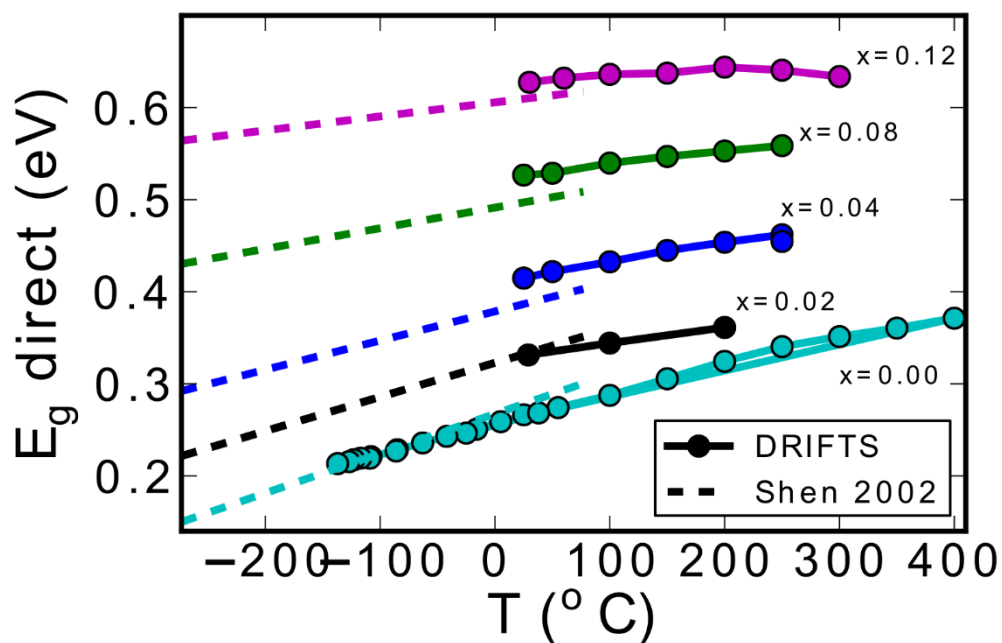


Figure 4-9: Temperature dependent optical band gap (direct extrapolation) in $(\text{PbSe})_{1-x}(\text{SrSe})_x$ from room temperature to $\sim 200^\circ\text{C}$ [174].

Ultimately, the optical properties are not critical to optimization of these materials, rather, they serve as a tool to help provide insight into the underlying band structure features which give rise to the measured electronic properties. Of all of the samples which we have measured, the ones with the highest peak zT (of all of the sodium doping levels for each Sr content, x) are shown in Figure 4-10. A large maximum zT is obtained of up to 1.5 at $T=900\text{ K}$ for the 8% SrSe sample, nearly 50% larger than the optimum zT for binary PbSe at this temperature. Largely, the enhancement is from the Seebeck coefficient (as is observed in the Seebeck Pisarenko plot, Figure 4-7d) as a result of a larger influence from the secondary bands at high doping levels rather than through thermal conductivity reduction through disorder scattering (as mentioned previously). At high temperatures, these effects are enhanced further because an even larger population of charge carriers develops in this high-degeneracy Σ band. In this case, the electronic properties confirm the existence of the secondary band even though optical measurements could

not isolate its contribution. The large zT enhancement in the alloyed samples illustrates the Σ band's importance for thermoelectric optimization in this system.

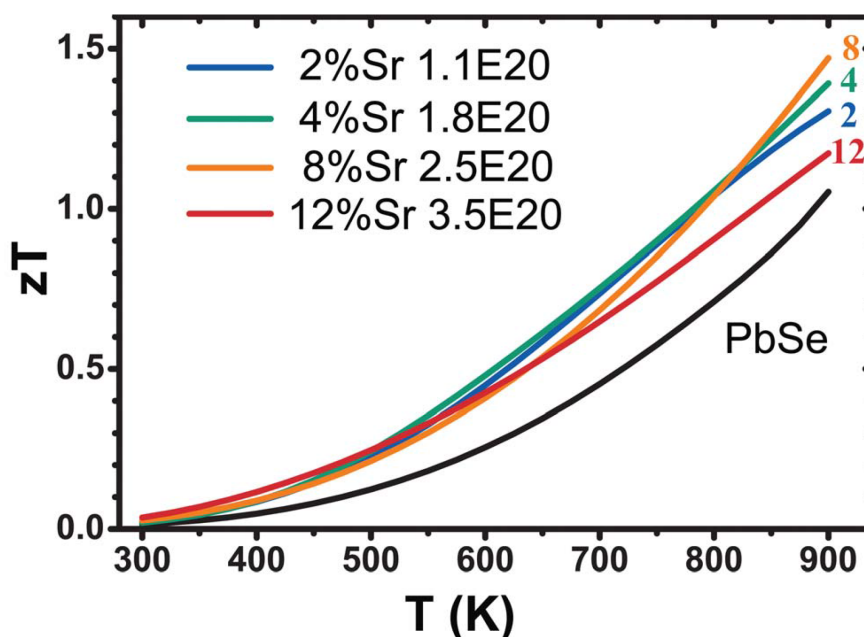


Figure 4-10: The observed zT of samples that have highest zT at 900 K and the corresponding Hall carrier densities at room temperature for $Pb_{1-x}Sr_xSe$ with different Sr content (zT for samples with different carrier density at each Sr content shown in supplementary), compared to the maximum zT evaluated for p-type PbSe.

4.3c - Conclusion

In this section, I presented a study of bulk $Pb_{1-x}Sr_xSe$ alloys with different x up to 12%. For each alloy composition, a p-type dopant, Na (K for two samples), is used to tune the carrier density for each Sr-content. The effect of Sr on band structure is revealed by transport and optical absorption edge measurements as well as first principle calculations. The band structure is sensitive to and gradually tunable with Sr content. Appreciable enhancement in thermoelectric performance was achieved and the maximum zT of 1.5 is found at 900 K (1.4 ± 0.1 in multiple samples with different compositions). Analysis further suggests that such enhancement is purely due to the change of band structure. This result provides a significant ($\sim 50\%$) enhancement over pure p-type PbSe, making an alloy which has performance comparable to that of binary p-type PbTe. It also shows how—even in a material that already has good thermoelectric properties, the

performance can be significantly enhanced through proper band structure engineering through doping and alloying.

4.3d - Methods

The samples are made via conventional melting and pressing route. Undoped samples in 25g batches were first made. To do so, high purity elements (Pb, 99.999%; Se, 99.999%; Sr, 99.9%) were loaded and sealed in carbon coated quartz ampoules, and then quickly melted for 15 minutes by induction heating. Each ingot was ground and hot pressed, and then sealed in another ampoule and annealed at 1073 K for 14 days. The doped samples of each alloy composition were made by reacting powder (3g) of undoped alloy with Na and Se at 1200 K for 5 days in sealed ampoules, and then hot pressed at 923 K. The disc samples for tests were 12.7 mm in diameter and about 1mm thick with density no less than 97% of theoretical value.

Modelling results shown in the Seebeck Pisarenko plot were obtained using many of the band engineering methods presented in Chapter 2. The density-of-states effective mass ($m_{d,L}^*$) of the light band and the conduction band is taken as $0.27 m_e$ at 300 K and changes with temperature following $\frac{d \ln(m_{d,L}^*)}{d \ln T} = 0.5$, the anisotropy factor K is taken as a constant 1.75 and the valley degeneracy was set to 4. The deformation potential for the conduction band and the light band were determined as 25 and 35 eV. Little is known for the parameters of the heavy band. Based on suggested values from Veis [127] and transport properties of p-type PbSe at high temperatures these parameters are determined to be $m_{d,\Sigma}^* = 4.2 m_e$, $K = 1$, $N_{v,\Sigma} = 12$, and $E_{def} = 28$ eV. The band gap and the gap between two valence bands change with temperature and Sr content ($\text{Pb}_{1-x}\text{Sr}_x\text{Se}$) following $E_g = 0.17 + 3 \times 10^{-4} T + 3x$ and $\Delta E = 0.32 - 2.2 \times 10^{-4} T - 1.5x$. The temperature dependence of E_g is based on results from the previous section on binary, undoped PbSe. The Sr-dependence of the band gap was determined from optical measurements at room temperature for the undoped Sr alloys. The temperature dependence of ΔE is based on Veis' optical

measurement result [127] and modeling of transport data of p-type PbSe at high temperatures, and its dependence on Sr content is taken assuming the band gap increase in $\text{Pb}_{1-x}\text{Sr}_x\text{Se}$ alloys is from the movement of two bands at L point simultaneously towards opposite directions (half of dE_g/dx , as mentioned previously). Alloy scattering of electrons was necessary to account for at higher Sr content. The alloy scattering potential, U , is taken as 3 eV for the light valence band, which is estimated from measured Hall mobility of undoped $\text{Pb}_{1-x}\text{Sr}_x\text{Se}$ alloys. The same U is taken for the conduction band because no data is available so far to estimate it more accurately. U for the heavy band is assumed to be 1.5 eV. A smaller U for the heavy band is consistent with the assumption that the heavy band position does not explicitly depend on Sr content. The value of 1.5 eV is used to provide the best overall fitting for all alloy compositions.

4.4 - Two Band Thermoelectric Performance in SnTe—Optimization Towards Single Band Behavior

4.4a - Introduction

As discussed in detail previously, the mechanism for p-type PbTe's outstanding thermoelectric performance is its complex valence band structure, especially at high temperatures where the energy of primary (L) and secondary (Σ) maximums are thought to be aligned, leading to extraordinarily high valley degeneracy[16]. In SnTe [128], one might also expect good thermoelectric performance because it shares many of the same characteristics with PbTe, specifically, both exist in the rock salt crystal structure and both have multiple valence bands [185] which contribute to the thermoelectric properties. However, unlike PbTe, SnTe is riddled with intrinsic defects which results in a heavily doped ($p \sim 10^{20}\text{--}10^{21} \text{ cm}^{-3}$) material and a mediocre zT (around 0.5 at 900 K)[129, 186]. Nonetheless, several works have confirmed the existence of two valence bands (as in PbTe) and have estimated their transport parameters[129, 130, 187-189].

SnTe has a large valence band offset, ΔE , of around 0.3-0.4 eV at room temperature, larger than PbTe, which is closer to 0.1 eV (Figure 4-11c) [90, 130]. The two valence bands in SnTe are known to give rise to a unique Seebeck coefficient behavior as the carrier concentration is varied (Seebeck Pisarenko relation). A minimum Seebeck coefficient is observed in the Pisarenko plot (Figure 4-11a) near $n_H=1-2 \times 10^{20} \text{ cm}^{-3}$, followed by a maximum at about $n_H=8 \times 10^{20} \text{ cm}^{-3}$. Theoretical calculations confirm the position of the two valence bands in k-space (at the L and Σ points as in the lead chalcogenides) and have provided some insight into their character [29, 190-193]. Other than thermoelectric properties, other works have discussed SnTe and its alloys with regards to their uses as long wavelength detectors [194-196], or most recently as topological insulators [191, 197, 198]. Similar to PbTe, SnTe has been studied rather thoroughly over the years for its thermoelectric properties, but in light of a recent resurgence in band-engineering in the lead chalcogenides it is worthwhile to take a closer look at the properties of SnTe as well, especially in regards to optimization of the carrier concentration.

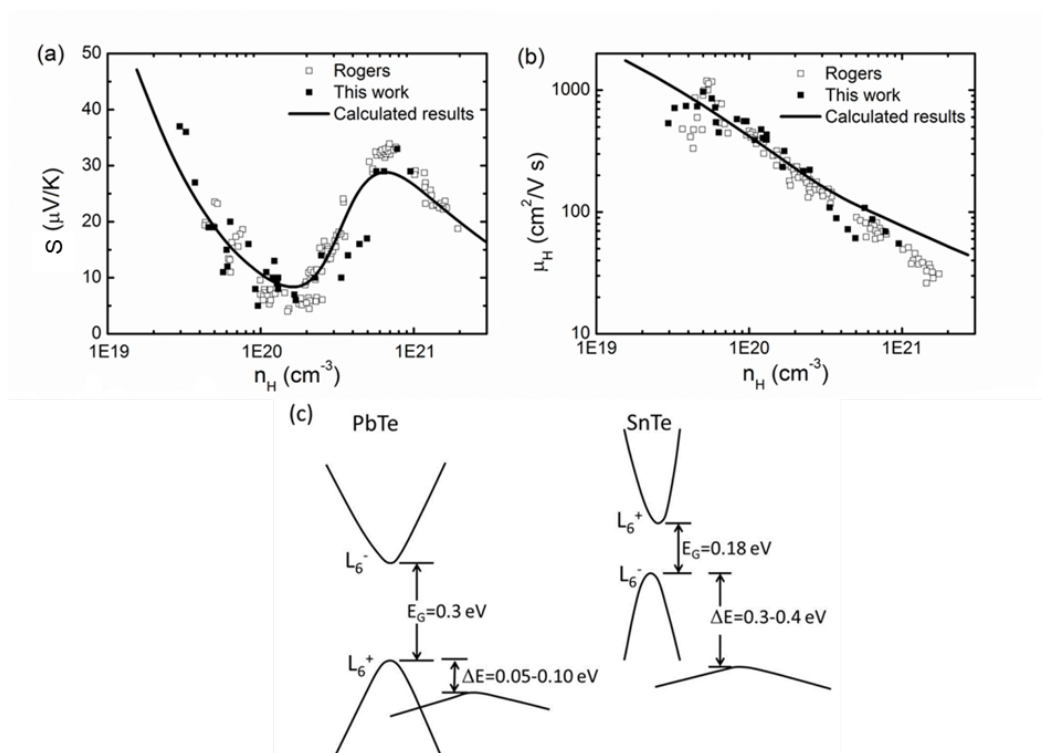


Figure 4-11: a) Seebeck coefficient and b) Hall mobility as a function of Hall carrier concentration at 300 K for $\text{SnTe}_{1-x}\text{I}_x$ and SnTe_{1+y} , $\text{Gd}_z\text{Sn}_{1-z}\text{Te}$. Solid squares are our experimental results, open squares are Rogers' reported results [130], solid curves are calculated from a two band model. c) A schematic diagram of the near edge band structure in PbTe and SnTe . (Rogers et al reported a band offset of 0.3 eV for SnTe . Our results yielded different fitting parameters, and we found that 0.4 eV was required for best fit.)

The unique Seebeck coefficient behavior of SnTe as the carrier concentration varies stimulates our interests to explore the nature of electrical transport in SnTe and to optimize the thermoelectric properties. Finding the optimum doping level in semiconductors with complicated band structures is crucial to obtaining a thermoelectric material with the optimum performance. In this work, I will show that both the Seebeck coefficient and zT value increase either by substituting donor (I) or acceptor (extra Te and Gd) dopants. We observe that the peak zT value ($zT_{\text{max},1}=0.6$ at 673 K) of I-doped SnTe with decreased carrier concentration ($3 \times 10^{19} \text{ cm}^{-3}$) is higher than the other peak zT value of extra Te or Gd-doped SnTe ($zT_{\text{max},2}=0.4$ at 773 K) with increased carrier concentration ($6 \times 10^{20} \text{ cm}^{-3}$), suggesting that the light, primary valence band is most important in these systems. This unique behavior is contrary to the behavior in the lead chalcogenides where the second, heavy band usually leads to improved figure of merit. I would like to acknowledge contributions to this work from Min Zhou, who was an equally contributing author on the original paper [128].

4.4b - Results and Discussion

The measured Hall carrier concentration ($p_H=1/eR_H$) of $\text{SnTe}_{1-x}\text{I}_x$, SnTe_{1+y} , and $\text{Gd}_z\text{Sn}_{1-z}\text{Te}$ samples at 300 K are shown in Figure 4-12. The Hall carrier concentration of stoichiometric SnTe was found to be around $1.1 \pm 0.2 \times 10^{20} \text{ cm}^{-3}$ at 300 K when prepared by using the described method. This value is slightly lower than Zhang's report (about $2 \times 10^{20} \text{ cm}^{-3}$) [199]. Extra Te is thought to induce cation vacancies which act as double acceptors [58, 200]. Brebrick, whose data is also shown in Figure 4-12a, studied closely Te solubility in SnTe and concluded that the phase width always leaned towards the Te rich side due to Sn vacancies; this phase width leads the heavily p-type character of intrinsic

SnTe. Our work agrees with the cation vacancy mechanism and yields ~ 1.7 holes per Te atom, although Brebrick saw more (3 holes per Te atom) [129]. Because Brebrick used carefully controlled and measured data for Te content while we use nominal composition only, Te loss through vaporization during synthesis is a plausible explanation of the difference. Dopant solubility in SnTe has been thoroughly studied by Rogacheva et al.; they investigate the complexities involved with doping phases that are intrinsically nonstoichiometric [201].

Gd with normal valence Gd^{3+} might be expected to substitute for Sn^{2+} and be an electron donor, but instead Gd is observed to cause an increase in p-type, hole carrier concentration. Similar results were reported by Story et al., who suggest that Gd is a resonant dopant; however, no Seebeck increase was observed relative to Te-doped samples which would indicate resonant states, probably due to a lower Gd content ($<1\%$) and higher temperatures than used by Story et al. [202] While the exact mechanism of Gd doping is not clear, the Gd-doped samples showed a linear increase in n_H with Gd doping for $z > 0.0025$.

We also attempted to counter dope SnTe by substituting Te with Iodine. While much work has been done on cationic substitutions, far fewer works study how SnTe is affected by anion substitution. As pointed out by Rogacheva et al, the cationic dopants that have the highest solubility are those which have similar ionic radii to Sn. Hence, Iodine (which has a similar ionic radius to Te) should be a good candidate for anionic substitutional doping in SnTe. As observed in Figure 4-12b, the carrier concentration linearly decreased to as low as $3 \times 10^{19} \text{ cm}^{-3}$ with $\sim 40\%$ doping efficiency, assuming that one electron is donated per iodine atom. The doping efficiency appears linear until $N_I \sim 25 \times 10^{19} \text{ cm}^{-3}$ ($x = 0.015$), where the carrier concentration continues to decrease, but at a slower rate. The observed carrier concentration has been achieved by previous authors [203-205], but their

interpretation of it and its significance to the thermoelectric properties was not thoroughly studied.

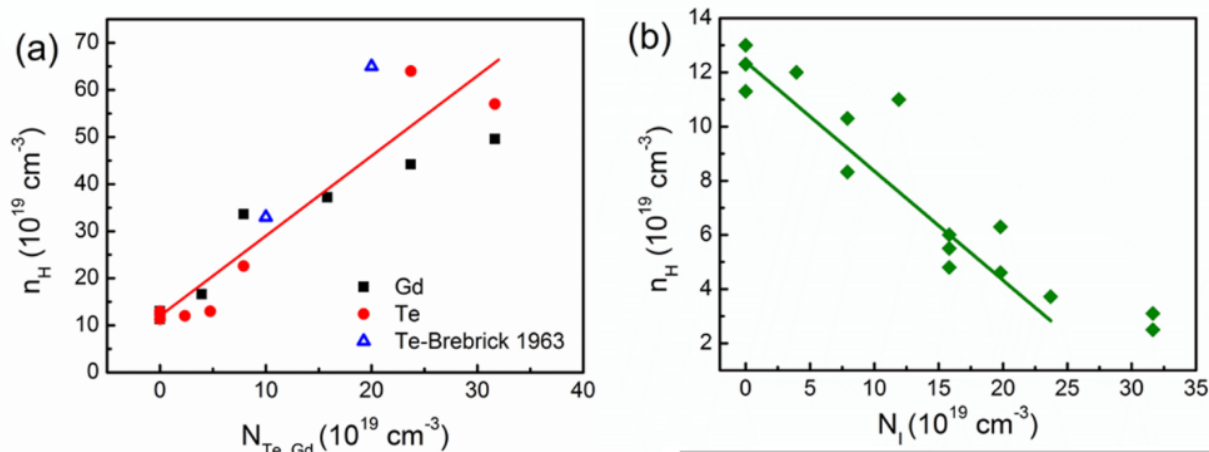


Figure 4-12: Hall carrier concentration as a function of dopant concentration a) Gd, Te excess as acceptors, b) I as donor. Solid lines represent guides to the eye for our data and correspond to 1.7 holes per atom for the Gd/excess Te case shown in a, and 0.4 electrons per Iodine atom as in b.

The measured temperature dependent transport data for samples with nominal composition $\text{SnTe}_{1-x}\text{I}_x$, $\text{Gd}_z\text{Sn}_{1-z}\text{Te}$, and SnTe_{1+y} are shown in Figure 4-13. Stoichiometric SnTe data reported by Zhang et al (green dashed lines for samples with a slightly different n_H than SnTe in this work) are also shown. Degenerate semiconducting behavior, indicated by an increasing Seebeck coefficient and resistivity with temperature, is observed for all samples. As the iodine content is increased, the measured Seebeck coefficient and electrical resistivity increase, consistent with the decrease of Hall carrier concentrations shown in Figure 4-12. This suggests that I atoms substitute for Te and supply extra electrons which compensate the effect of intrinsic Sn vacancies. Conversely, the p-type dopants (Gd and excess Te) reduce the resistivity, consistent with an increase in carrier concentration. The Seebeck coefficient for these samples, unlike in the I doping case, show an increase with increasing doping level at room temperature, which is a direct consequence of the two band behavior described in Figure 4-11. Further, the most heavily doped sample ($6 \times 10^{20} \text{ cm}^{-3}$) also has nearly the highest Seebeck coefficient at room

temperature, but it does not increase as much with temperature as samples with lower doping levels.

The total thermal conductivity and the calculated lattice thermal conductivity of $\text{SnTe}_{1-x}\text{I}_x$ samples are shown in Figure 4-13(e, f). The total thermal conductivity of the undoped SnTe decreases with temperature, reaching 2.3-3.0W/m K at 773K. The thermal conductivities of all the I-doped $\text{SnTe}_{1-x}\text{I}_x$ are lower than that of undoped SnTe, which comes from the reduction of electronic thermal conductivity as a result of a decreasing hole concentration. The lattice thermal conductivity, κ_L , is calculated by subtracting the electronic contribution ($\kappa_e = LT/\rho$) from the total thermal conductivity, where L is the Lorenz number that was estimated from a two-band model ($L = (L_L \sigma_L T + L_\Sigma \sigma_\Sigma T + \kappa_{bipolar}) / (\sigma_L T + \sigma_\Sigma T)$), where $\kappa_{bipolar} = T(\sigma_1 S_1^2 + \sigma_2 S_2^2 - (\sigma_1 S_1 + \sigma_2 S_2)^2 / (\sigma_1 + \sigma_2))$. The lattice thermal conductivity of all the I-doped $\text{SnTe}_{1-x}\text{I}_x$ samples decreased with temperature, and then increased when the temperature is over 600 K. This suggests that bipolar effects occur in I-doped $\text{SnTe}_{1-x}\text{I}_x$ samples with lower carrier concentrations at high temperature. κ_L is not shown for Te and Gd doped samples, which were shown to be additionally complex due to large contributions from the Σ band.

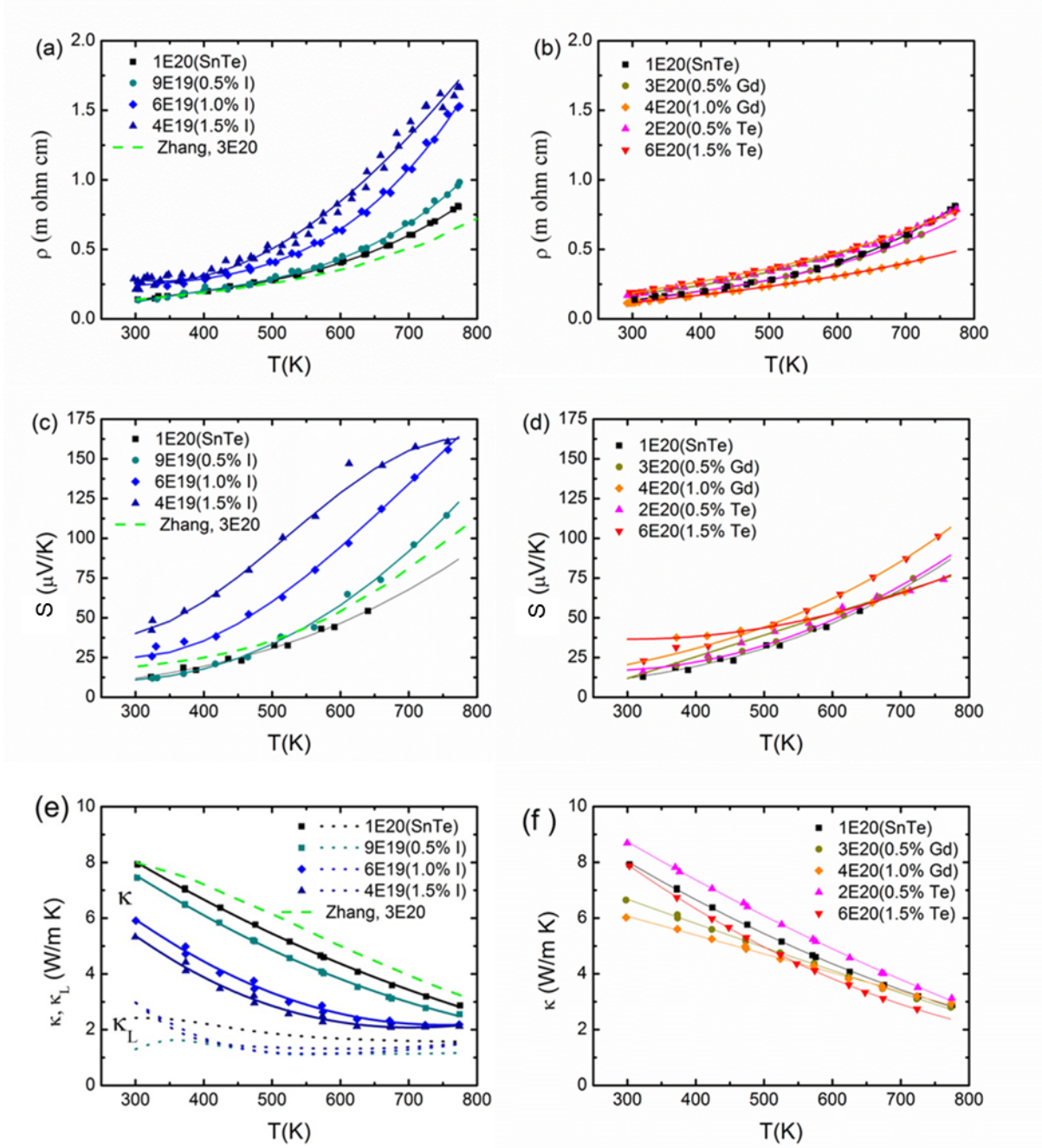


Figure 4-13: Thermoelectric transport properties for various SnTe samples: a) resistivity of SnTe and $\text{SnTe}_{1-x}\text{I}_x$, b) resistivity of SnTe, SnTe_{1+y} , and $\text{Gd}_z\text{Sn}_{1-z}\text{Te}$, c) Seebeck of SnTe and $\text{SnTe}_{1-x}\text{I}_x$, d) Seebeck of SnTe, SnTe_{1+y} , and $\text{Gd}_z\text{Sn}_{1-z}\text{Te}$, e) thermal conductivity and lattice thermal conductivity of SnTe and $\text{SnTe}_{1-x}\text{I}_x$, and f) thermal conductivity and lattice thermal conductivity of SnTe, SnTe_{1+y} , and $\text{Gd}_z\text{Sn}_{1-z}\text{Te}$. Legends indicate room temperature Hall carrier concentrations and a brief description of the samples as follows: $\text{SnTe}_{1-x}\text{I}_x$, $\text{Sn}_{1-x}\text{Gd}_x\text{Te}$, and SnTe_{1+x} for Iodine doped (a, c, e), Gd doped (b, d, f), and excess Te (b, d, f) samples, respectively. All plots show both raw experimental data (points) and polynomial fits (lines).

Full optimization of SnTe yields a higher zT (average and peak) for samples doped with Iodine. The thermoelectric figure of merit, zT , is shown as a function of temperature

in Figure 4-14 for Iodine, Gd, and Te rich samples along with results from Zhang et al for an undoped and an In doped sample[199]. We show that the undoped SnTe ($n_H = 1.1 \times 10^{20} \text{ cm}^{-3}$) shows low zT values over the measured temperature range yielding a maximum of 0.23 at 773 K. This is lower than the reported zT value (0.39) of intrinsic SnTe with a higher carrier concentration ($n_H = 2 \times 10^{20} \text{ cm}^{-3}$) at the same temperature from Zhang et al. (as shown in Figure 4-14a). From Figure 4-14a, zT values increased with donor I-dopant and a peak zT value of 0.6 was obtained for $\text{SnTe}_{0.985}\text{I}_{0.015}$ at 700 K, corresponding to an optimum doping level of around $4 \times 10^{19} \text{ cm}^{-3}$, which was the lowest attainable with iodine doping that did not lead to hysteretic behavior in the transport properties. zT values of 0.45-0.6 were obtained for several samples with room temperature n_H of $4.0\text{-}6.1 \times 10^{19} \text{ cm}^{-3}$. This means that decreasing carrier concentration is a valid approach to optimize zT of SnTe by doping with iodine.

Alternatively, zT values increased with acceptor Te or Gd-dopant also. The other peak zT value of 0.4 was obtained for the most heavily doped samples ($\text{Gd}_{0.01}\text{Sn}_{0.99}\text{Te}$ and $\text{SnTe}_{1.015}$, $n_H = 4\text{-}6 \times 10^{20} \text{ cm}^{-3}$) at 773K, which is about 30% lower than the iodine doped samples. Unlike conventional single band behavior, we show that both I-doped SnTe and Gd-doped SnTe have higher zT values than that of stoichiometric SnTe. Figure 4-14c shows the average zT value ($\overline{zT} = \frac{\int_{300}^{773} zT dT}{773-300}$) of I-doped and Te-rich SnTe samples along with Zhang et al. $\text{In}_{0.0025}\text{Sn}_{0.9975}\text{Te}$ samples over the temperature range of 300-773 K. $\text{SnTe}_{1.015}$ shows an average zT of 0.15, but the average zT value of best I-doped SnTe (0.35) is about the same as the best In-doped sample (0.32) that contains resonant states. This indicates that the low-temperature zT value in I-doped samples is quite a bit higher than either the intrinsic or In-doped samples from Zhang et al.

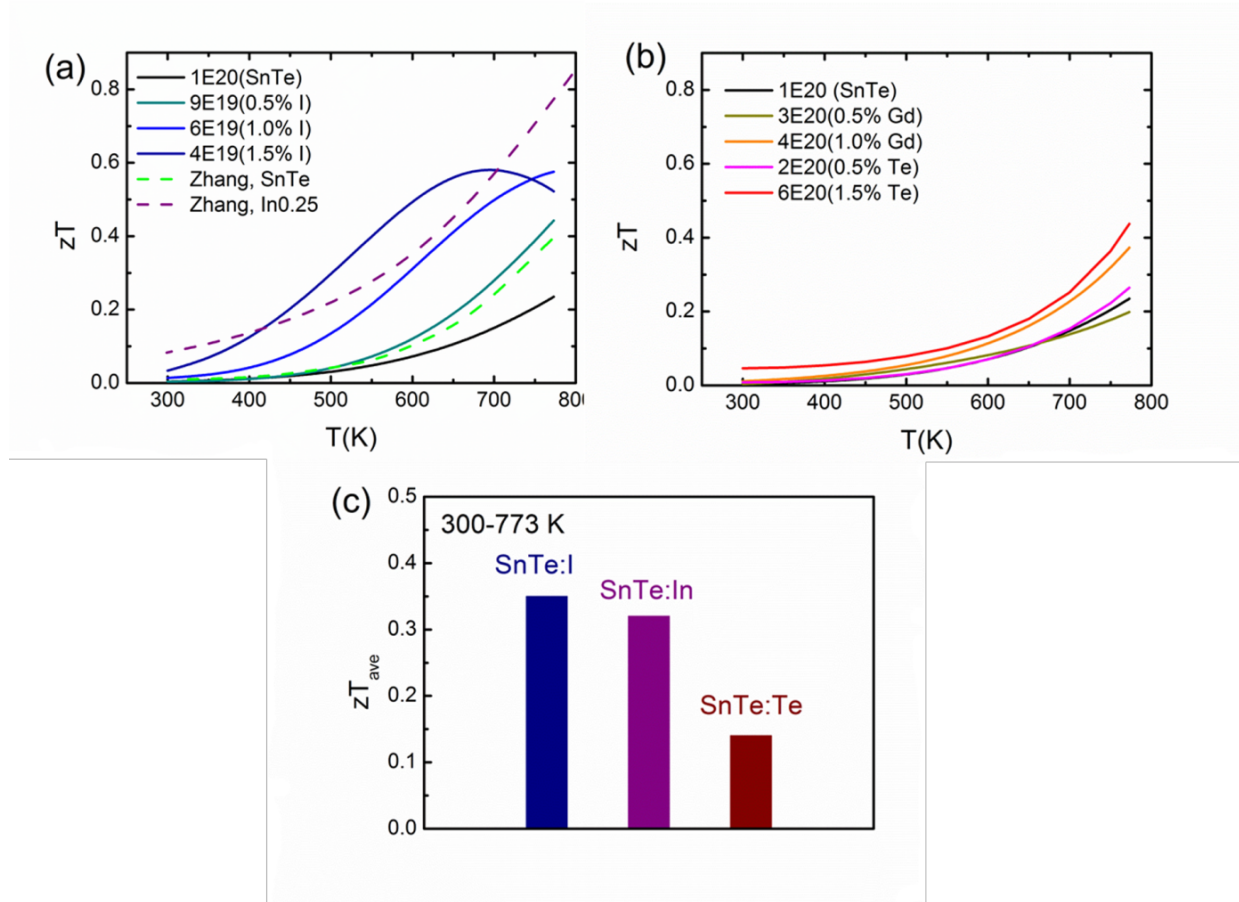


Figure 4-14: a) zT of $\text{SnTe}_{1-x}\text{I}_x$ as function of temperature, data (dashed lines) are from the literature [199]. b) zT of SnTe_{1+y} and $\text{Gd}_z\text{Sn}_{1-z}\text{Te}$ as function of temperature. c) The average zT between 300 and 773 K for optimally doped samples; data of SnTe:In are from the literature [199]. zT estimates are obtained from polynomial fits of transport data in Figure 3.

The Seebeck coefficient as a function of Hall carrier concentration (Pisarenko plot) is shown in Figure 4-11a for $\text{SnTe}_{1-x}\text{I}_x$ and SnTe_{1+y} , $\text{Gd}_z\text{Sn}_{1-z}\text{Te}$ at 300 K along with reported results from Brebrick and Rogers et al. [129, 130]. The plot shows a unique, non-monotonic n_H dependence brought about by the two interacting valence bands. For carrier concentration of $1\text{-}2 \times 10^{20} \text{ cm}^{-3}$, the Seebeck coefficient shows a minimum value of about $5\text{-}10 \mu\text{V/K}$. The Seebeck coefficient then increases to a maximum of about $30 \mu\text{V/K}$ at carrier concentration of $6\text{-}8 \times 10^{20} \text{ cm}^{-3}$. Figure 4-11b shows the relationship between the carrier mobility and Hall carrier concentration of all the samples as well as data reported by Rogers et al. at 300 K [130]. The carrier mobility of stoichiometric SnTe is about 400-

500 cm²/V-s at room temperature and always decreases with increasing carrier concentration for all SnTe_{1-x}I_x and SnTe_{1+y}, Gd_zSn_{1-z}Te samples. The experimental data of both Seebeck coefficient and mobility are fitted by a two band model (the solid curve) using a Kane band (SKB) for the L and a parabolic band (SPB) for the secondary Σ valence band (as described in detail in the Methods section later in this chapter).

As shown in Figure 4-15, the high temperature Seebeck coefficient and carrier mobility could also be explained by the same model, with the valence band offset (ΔE) and band effective masses allowed to change as fitting parameters as a function of temperature. The non-monotonic behavior for the Seebeck coefficient becomes less significant at high temperature (Figure 4-15a), probably a result of a broadening Fermi distribution and temperature dependent shifts in the band structure. By fitting experimental results we determine that the density of states effective mass m_L^* of the L valence band is 0.14 m_e for SnTe_{1-x}I_x at 300 K, and it changes with temperature roughly according to $d\ln m_L^*/d\ln T=0.55$. Similar temperature dependence has been reported in other IV-VI compounds with similar band structure [16, 65, 206]. Little is known about the parameters for the heavier, Σ band, and they are difficult to determine directly using experimental techniques. As a result, they were adjusted to fit the experimental Seebeck and mobility data. The density of states effective mass m_H^* was fit to be 1.7 m_e at 300 K, and it changes with temperature according to $d\ln m_H^*/d\ln T=0.5$. The 300K values are comparable to those reported by Brebrick et al. [129]. The valence band offset energy, ΔE , between the two bands was found to be 0.4 eV at 300 K according to the fitting result; the best fit of the data required ΔE to decrease roughly linearly with temperature at a rate of 3.4×10^{-4} eV/K (similar to the lead chalcogenides in the previous sections). I should note that these values are likely not unique, and that similar fits could also be performed with different sets of parameters.

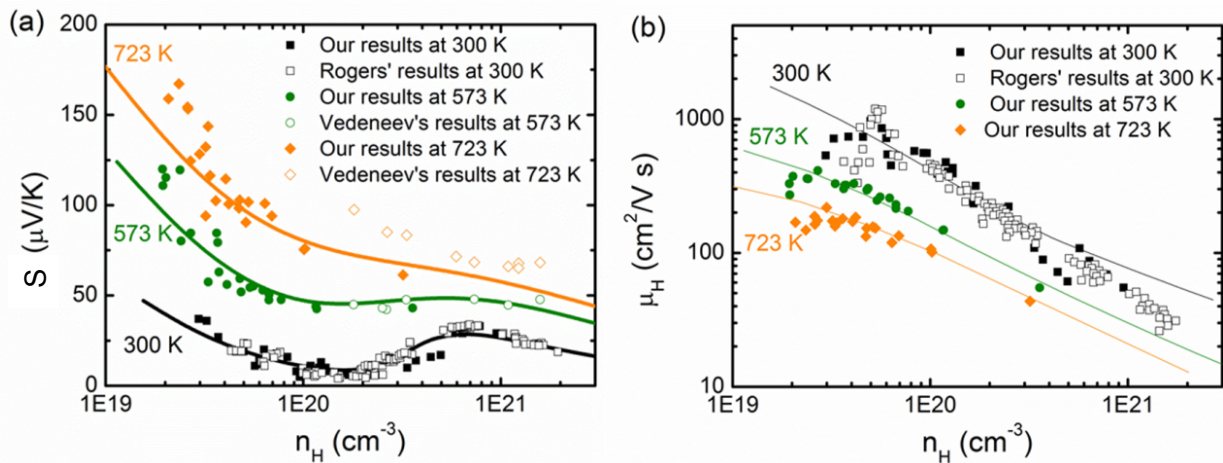


Figure 4-15: a) Seebeck coefficient and b) Hall mobility as a function of Hall carrier concentration at different temperatures. Solid symbols represent our experimental results, open symbols correspond to literature data (Vedeneev {Vedeneev, 1998 #9388} and Rogers {Rogers, 1968 #9294}). Each is presented at three temperatures: 300, 573, and 723 K, which are given by squares, circles, and diamonds, respectively. Solid curves represent the results of the two band model.

Figure 4-16 shows zT as a function of Hall carrier concentration for $\text{SnTe}_{1-x}\text{I}_x$, SnTe_{1+y} and $\text{Gd}_z\text{Sn}_{1-z}\text{Te}$ samples at different temperatures. Note that a local minimum exists in zT vs. n_H for temperatures of 300 and 600 K, which corresponds to a carrier density of $\sim 1 \times 10^{20}$ cm⁻³, approximately the composition of stoichiometric SnTe. At a higher temperature of 773 K, the model predicts a single maximum in zT as seen in most thermoelectric materials, but the peak is broadened due to the increasing influence of the second band. From Figure 4-16, both the experimental and model results indicate a significant zT increase with decreasing carrier concentration, yielding a maximum in the $10^{18} - 10^{19}$ cm⁻³ range. In this work, the solubility of I in $\text{SnTe}_{1-x}\text{I}_x$ ($x = 0.015$, $n_H \sim 4 \times 10^{19}$ cm⁻³) has limited us from achieving the optimized n_H for the predicted maximum zT to be obtained (which requires $n_H \sim 8 \times 10^{18}$ cm⁻³). While we do expect bipolar effects to begin to play a role at low doping levels and high temperatures, which is not accounted for in this model, the conclusions remains that optimizing SnTe carrier concentration towards the light band results in significant improvement.

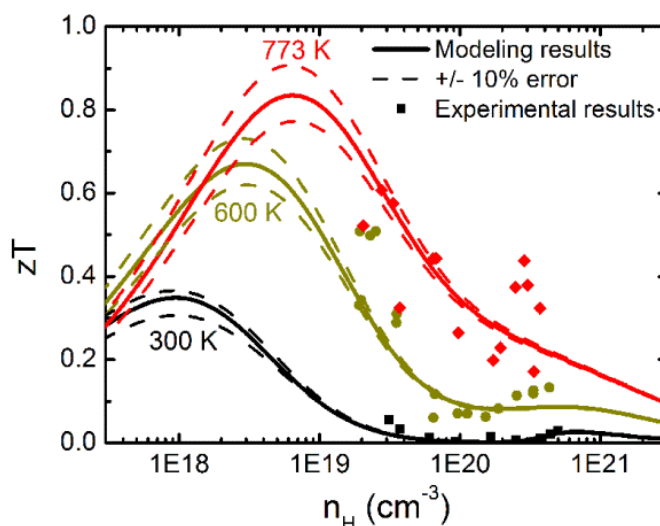


Figure 4-16: zT as a function of Hall carrier concentration for $\text{SnTe}_{1-x}\text{I}_x$ and SnTe_{1+y} , $\text{Gd}_z\text{Sn}_{1-z}\text{Te}$. Solid curves are modeling results, and dashed lines are uncertainty values for the model zT which account for a $\pm 10\%$ error in κ_L . The calculated lattice thermal conductivity of $2.5 \pm 10\%$ W/m K (300 K), $1.23 \pm 10\%$ W/m K (600 K), and $1.0 \pm 10\%$ W/m K (773 K) were used in the zT calculation as obtained from I-doped samples (Figure 3e).

While both SnTe and PbTe are IV-VI materials have the same crystal structure and similar electronic band structures, their thermoelectric performance and optimization strategies are quite different. At first, one might write off SnTe due to its large intrinsic defect concentration and higher lattice thermal conductivity when compared to PbTe. However, this work suggests that it does in fact give a reasonable zT when optimizing towards the low carrier concentration light band rather than the heavier Σ band; this is achieved by doping with iodine. While valley degeneracy and band convergence play a crucial role in the high zT for PbTe (more than 1.5 at $T \sim 800$ K), the larger band offset in SnTe (0.4 eV for SnTe versus 0.1 eV for PbTe at 300 K) makes convergence unattainable in SnTe for temperatures below its melting point. In addition, the thermoelectric quality factor [18, 65], B (Equation 2-6), can be used to determine the quality for the L and Σ bands to be 0.42 and 0.27, respectively, in SnTe at 600 K. The light band is estimated to have nearly 50% higher quality factor than the heavy band in this system due primarily to the low band mass (and corresponding high mobility). Coupled with a large band offset (~ 6

$k_B T$ at 600 K), the peak zT for SnTe occurs for a chemical potential near to the light valence band edge. This is in contrast to PbTe where the heavy band is believed to have as good or better quality factor than the light band with a much smaller band offset ($\Delta E \sim 1.5 k_B T$ at 600 K) [18]. So, while valley degeneracy and the heavy band at Σ play an important role in PbTe [16], they are not viable options for improving zT in SnTe.

While intrinsic SnTe seems to have too large of band offset to utilize the heavy band, several successful attempts at band engineering have been achieved. Tan reported a high zT of 1.3 for Cd-doped [170] and Hg-doped [169] SnTe, which they attribute to changing ΔE from the addition of Cd/Hg and nanostructuring. Han and Chen et al reported zT of 0.9-1 for SnTe-AgSbTe₂ alloys [207, 208]. These latest works are encouraging in terms of making a useful thermoelectric device that is lead free.

4.4c - Conclusion

While undoped SnTe has very poor thermoelectric performance, SnTe can be greatly improved through carrier density tuning. We have shown that by either increasing or decreasing the carrier concentration, the zT can be improved relative to naturally synthesized, nominally undoped SnTe. A peak zT value of 0.6 is obtained for SnTe_{0.985}I_{0.015} sample with a lower carrier concentration of $4 \times 10^{19} \text{ cm}^{-3}$, which is about 50% higher than the other peak zT value of 0.4 for SnTe_{1.015} with a higher carrier concentration of $p_H = 6 \times 10^{20} \text{ cm}^{-3}$. Transport property models predict higher zT if the carrier concentration could be reduced further to $1 \times 10^{19} \text{ cm}^{-3}$. Different from In-doped SnTe that alters the host band structure, this work revealed the inherent merit of SnTe thermoelectric materials. With further band engineering SnTe may become an efficient lead free alternative to lead chalcogenide thermoelectric materials.

4.4d - Methods

Polycrystalline samples of SnTe_{1-x}I_x ($0 \leq x \leq 0.02$), SnTe_{1+y} ($0 < y \leq 0.015$), Gd_zSn_{1-z}Te ($0 < z \leq 0.02$) were prepared by using a melt alloying and hot pressing technique. Pure

elements and TeI₄ (Sn, 99.999%; Te, 99.999%; Gd, 99.99%; TeI₄, 99.999%, ultra dry) were weighed out according to each composition and loaded into quartz ampoules, which were then evacuated and sealed. The sealed ampoules were slowly heated to 1273 K and kept for 24 h followed by water quenching. The ingots obtained were further annealed at 973 K for 120 h before being crushed and ground into fine powders. The powders were then hot pressed at 823 K under 1 atm argon with 40 MPa pressure for 30 min. A typical disc shaped sample obtained is 12 mm in diameter with density no less than 95% of theoretical density (6.46 g/cm³). Electrical properties were measured as detailed in Chapter 2. The heat capacity, C_p , was determined from: $C_p = C_{p,300} + C_{p1} \times ((T/300)^\alpha - 1) / ((T/300)^\alpha + C_{p1}/C_{p,300})$ [209], where T is the absolute temperature, $C_{p,300}$ is the specific heat capacity at 300 K. For SnTe, $C_{p,300}$ is 0.1973 J/g K, C_{p1} is 0.115 J/g K, α is 0.63 [209].

A two-band model was used for modeling the light and heavy bands to explain thermoelectric transport properties. Transport properties were modeled following the procedures outlined in previous work [65, 210] and in Chapter 2 of this thesis. The light and heavy valence band properties were calculated by evaluating the full generalized Fermi integrals as a function of chemical potential. The L band was assumed to be a nonparabolic, Kane band, with a nonparabolicity parameter, β , given by $k_B T / E_g$, where E_g was assumed constant at 0.18 eV [211], while the Σ band was modeled as a parabolic band. More specific details of the modelling results can be viewed in the supplementary material of a paper published on this subject [128].

4.5 - Conclusions

IV-VI materials have proven to have a breadth of interesting and measureable band structure properties which can be used for building world-class thermoelectric materials. In this chapter, I have shown that by using a combination of optical and electronic properties measurements coupled with *ab-initio* calculations we can gather a wealth of information about the electronic band structures in the IV-VI materials. In Section 4.2, I have provided new

optical/computational evidence of the convergence temperature in the lead chalcogenides which suggests that convergence occurs at ~ 700 K in PbTe, much higher than the commonly cited result that claims (~ 400 K). These experimental results have helped to aid band engineering strategies by providing the data needed to accurately model the band structure at high temperatures. Section 4.3 shows a successful band engineering study in PbSe/SrSe alloys which leads to $\sim 50\%$ enhancement (max zT of 1.5) relative to the binary PbSe. In Section 4.4, two band transport behavior in SnTe is characterized in a doping study; here we determine that the zT in SnTe can be greatly improved upon decreasing the carrier concentration through iodine doping. My results have expanded upon the current literature by providing band structure properties in the IV-VI materials, allowing a clearer path towards proper optimization. The techniques learned here are generally applicable to other multi-band systems as well, and several will be discussed later in this thesis.